# HURST EXPONENT FOOTPRINTS FROM ACTIVITIES ON A LARGE STRUCTURAL SYSTEM

Vikram Pakrashi*
*Department of Civil and Environmental Engineering,School of Engineering, University College Cork, Cork, Ireland*
*v.pakrashi@ucc.ie*

Joe Kelly
*Roughan & O' Donovan Consulting Engineers,Arena House, Arena Road, Sandyford, Dublin, Ireland*
*Joe.Kelly@rod.ie*

Julie Harkin
*Roughan & O' Donovan Consulting Engineers,Arena House, Arena Road, Sandyford, Dublin, Ireland*
*jharkin06@qub.ac.uk*

Aidan Farrell
*National Roads Design Office, Maudlins, Naas Kildare, Ireland*
*afarrell@kildarenrdo.com*

* Corresponding Author
*Address:* Department of Civil and Environmental Engineering, School of Engineering, University College Cork, Cork, Ireland
*Email:* v.pakrashi@ucc.ie
*Phone*: 00353 857394824
*Fax*: +353 (0)21 427 6648

**Abstract**

This paper presents Hurst exponent footprints from pseudo-dynamic measurements of significantly varied activities on a damaged bridge structure during rehabilitation through continuous monitoring. The system is interesting due to associated uncertainty in large-scale structures and significant presence of human intervention arising from fundamentally different processes. Investigation into the variation of computed Hurst exponents on time

series of limited lengths are carried out in this regard. The Hurst exponents are compared with respect to specific events during the rehabilitation, as well as with the locations of collection of data. The variations of local Hurst exponents about the values computed for each activity is presented. The scaling of Hurst exponents for different activities are also investigated, which are representative of the extent of multifractality for each event. The extent of multifractality is assessed along with its source and time dependency.

Keywords: Hurst Exponent, Multifractal, Human Activity, Structural Systems, Uncertainty, Bridges

## 1. Introduction

The application of Hurst exponent is gaining considerable attention in recent times [1-5] in very disparate fields. The popularity of such application is not just related to the dependency on output data and the ease of application, but is often driven by the fundamental complexity in the nature of the application or the complexity in data itself. Investigations into the interpretation of computed Hurst exponents have already generated a significant body of research [6- 9] and still continues to do so. On the other hand, the methodology of computing or estimating the Hurst exponent [10-12], properties of Hurst exponent [13], along with related links to the multifractality of systems [14] remain extremely topical.

Independent of the varied methodology or interpretation, the estimated Hurst exponent values have been observed to have a potential to become a powerful tool for detection and estimation of features of interest from time series data. In this regard, applications on financial markets [15-16], oil prices [17], hydrology [18] and earthquake [19] have been reported and there exists an obvious popularity of applied problems that are related to the financial market. Estimation of future values [20-21] and rapid changes [22-24], detection of

influence of variables [25] or prediction of relationships between variables [26-27] have been studied in this regard. Most of the applications or detections deal with natural systems or financial systems, where the governing laws for the entire system are often too complex to model. A Hurst exponent based approach is extremely useful when a wide range of underlying activities exist within a system over a measured length of time, but the measurement from the system is not suitable for Fourier analysis based [28,29,30] or time-frequency analysis based [31,32,33,34,35,36] (wavelets, S-transform, Hilbert-Huang transform etc.) methods. Fourier based approaches are not very useful for data sampled at a very low rate [37] or when the contribution of certain frequencies is dominant only within a short period of time due to the integration carried out over the entire time domain. Windowed Fourier transforms, or in general, time-frequency type analysis like wavelets are better for application, but problems related to low sampling rate [38], uneven sampling rate [39] and masking [40] remain. The Hurst exponent based approach, even when the exponents may not have a strict interpretation, can have significant advantages for monitoring activities when collected data are not well sampled and are available without the knowledge of the system.

This paper investigates a system where varied natural and human activities on a large structure over a significant period of time generate the time series. The rehabilitation of an impact damaged full scale bridge structure was continuously monitored at multiple locations in this regard. The activities during the rehabilitation process were fundamentally different, and significant uncertainties related to the loading process were associated with the system, including human factors. The interaction can be viewed as that between planned human activities and designed systems exposed to environmental variables. The Hurst exponent signature related to such activities is investigated over time and at multiple locations. The potential of using Hurst exponent as a marker for changing activities or for structural health monitoring is investigated.

The rest of the paper is organised as follows: Section 2 describes the system and the data obtained from continuous monitoring; Section 3 briefly presents the methodology behind the estimation of Hurst exponent; Section 4 presents the results where the variation of Hurst exponents based on events and on the location of data collection is investigated, along with their variability and discussions on the implications of the results and Section 5 provides the conclusions of this investigation.

## 2. Experimental Details and Description of Data

The data was obtained from the emergency rehabilitation of an impact damaged bridge over a National Primary road of Ireland. The damage was due to an impact to the soffit from a low-loader carrying an excavator passing underneath the bridge. The two-span continuous slab – girder bridge comprises of six precast prestressed U8 type concrete beams connected by a continuity diaphragm. The reinforced concrete piers are integral to the deck and the ends of the bridge are simply supported on reinforced concrete abutments. Figure 1 presents a close-up photograph of this damage. Unknown redistribution of stresses took place following the impact. Hammer tapping and acoustic emission tests established that the true damage was more extensive than the apparently observed damage.

Figure 1. Apparent damage due to impact. The true damage is more extensive than this in depth and breadth.

The rehabilitation was carried out by preloading the bridge to 120 ton over the carriageway and at the two ends of the damage using concrete blocks at 20t increments. Hydrodemolition and removal of damaged concrete was carried out next. The preloading removed some of the tensile prestress from the top and also helped developing some prestrain at the location of damage. It also helped avoid damage due to sudden release of locked-in strains from damaged concrete. Following hydrodemolition, rapid-hardening and high-strength repair material was applied to the damaged region and the preloads were removed after the hardening of repair material. The removal of preload was expected to reintroduce some amount of lost prestress in the repaired zone. The structure was monitored throughout the rehabilitation process using pseudo-dynamic measurements of one sample every minute using vibrating wire strain gauges. Nineteen gauges were instrumented on the damaged bridge at five locations, referred to as Monitoring Points (MP). The low sampling frequency is related to the practical implementation of measurements at large scale. The choice is guided by the sampling resolution, robustness against physical activities and exposures to environmental and mechanical conditions and accuracy of collected data. A higher sampling frequency usually corresponds to small gauges that are easily affected by small electrical, mechanical and environmental fluctuations and lead to a lower quality of data with associated noise and fluctuations that are very difficult to estimate. From an implementation perspective, the connection with the large structure also is not very good due to the small size of the gauges and the rough surface of large structures. Additionally, these gauges with higher sampling frequency are not very robust against activities carried and the probability of losing the operational capability of significant number of gauges is unusually high. Although the

vibrating wire strain gauges used for the study have a low sampling rate, they provide reliable measurements and good resistance against activities with a low rate of sensor defect during monitoring periods. The connection with the structure is also good. Consequently, these types of gauges were considered to be better for large scale monitoring than the ones with a higher sampling frequency.

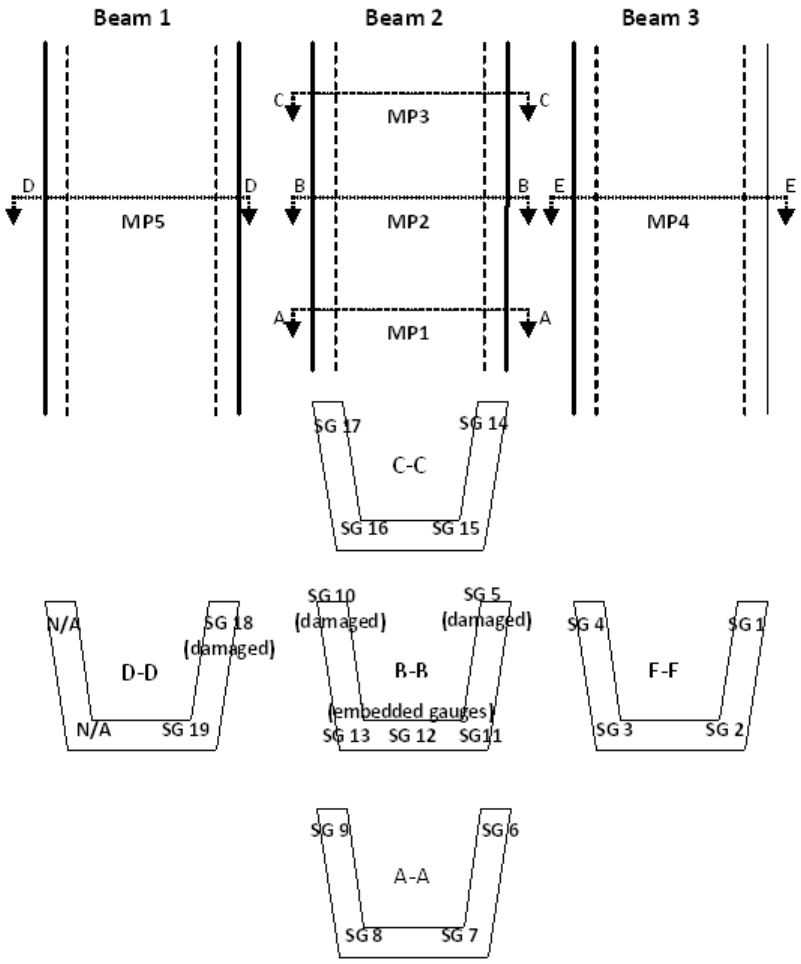


Figure 2a. Schematic of strain gauge arrangement on bridge during rehabilitation.

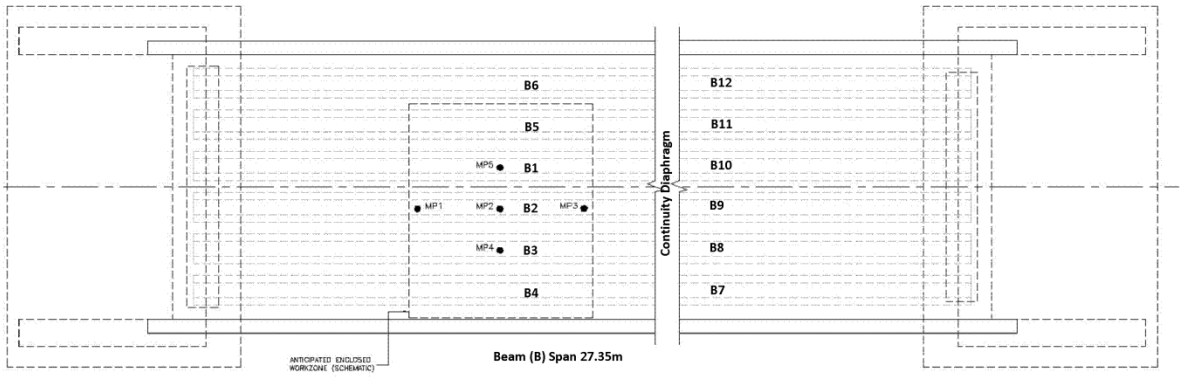


Figure 2b. Schematic of beam arrangement in plan view.

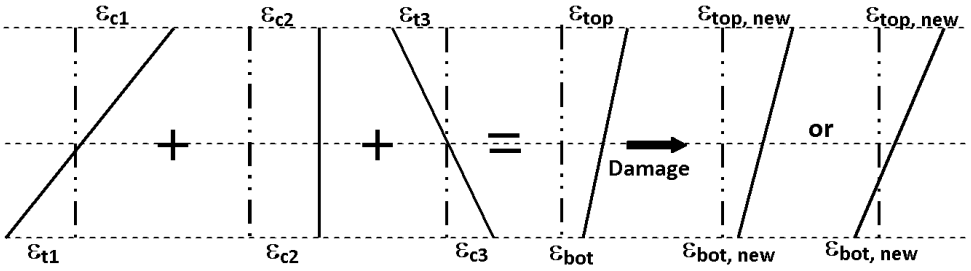


Figure 2c. Qualitative strain diagrams before and after damage.

Figure 2d. Removal of preloading following repair.

Figure 2a provides the schematic of the strain gauge (denoted as SG) arrangement on the bridge. Three of the nineteen gauges were embedded to the exposed tendon at the soffit of the

damaged beam (Beam 2). Three of the five Monitoring Points (MP1, MP2 and MP3) were located at the midpoint and at the two ends of the damage respectively while the other two were located on the two adjacent beams. The gauges were simultaneously zeroed and readings were automatically logged for all of the gauges every minute. Before the rehabilitation stage started, the structure was monitored under relatively quiescent conditions, during which the main action on the structure was thermal, due to the diurnal temperature variation. The structure was also monitored for some time after the rehabilitation during which some strength gain and strain redistributions are expected to occur along with thermal effects. Some of the gauges were damaged during the rehabilitation process at different times. Figure 2b presents a sketch plan of the bridge with the beams (B) indicated and the span of the beam mentioned. The monitoring points are also identified in the plan view. The beam numbers are unchanged from their original identification during the rehabilitation works. Figure 2c presents the qualitative strain diagram of the damaged beam before and after damage. Before damage, the simply supported beam experiences tension at bottom ($\varepsilon_{t1}$) and compression on top ($\varepsilon_{c1}$) from operational loads like self-weight, weight of superimposed road surfacing and vehicular passage. However, because the beams are prestressed, there exists a uniform compressive strain over the cross-section of the beam ($\varepsilon_{c2}$). Additionally, the centre of gravity of the compressive prestressing forces from the tendons are located at an eccentricity with respect to the neutral axis of the beam geometry in a way such that the moment due to the eccentricity creates some compression at bottom ($\varepsilon_{c3}$) and tension on top ($\varepsilon_{t3}$). When combined, these stresses tend to cancel out each other and ideally, through design, are expected to create a situation where the entire section is subjected to non-uniform compression within the compressive limit of concrete, thereby removing possibilities of tension cracks. Unknown stress re-distributions occur after damage and it is expected that the bottom compression is shifted more towards the tension zone, while the top is subjected to a

higher level of compression. It is also possible for the bottom to go into compression. The situation is further aggravated during rehabilitation due to removal of concrete. Figure 2d is presented to illustrate the repair carried out. A preload was applied on either side of the damage, introducing further tension and bottom and compression on top. The damaged section was repaired and when the repaired material hardened, the removal of prestressed attempted to regain some part of prestressing back into the cross-section. The extent of redistribution of stresses following preload removal is difficult to assess.

Figure 3 presents the data from two representative gauges with identified zones of time during which the activities carried out on the structure changed significantly. The strain readings are in microstrain units.

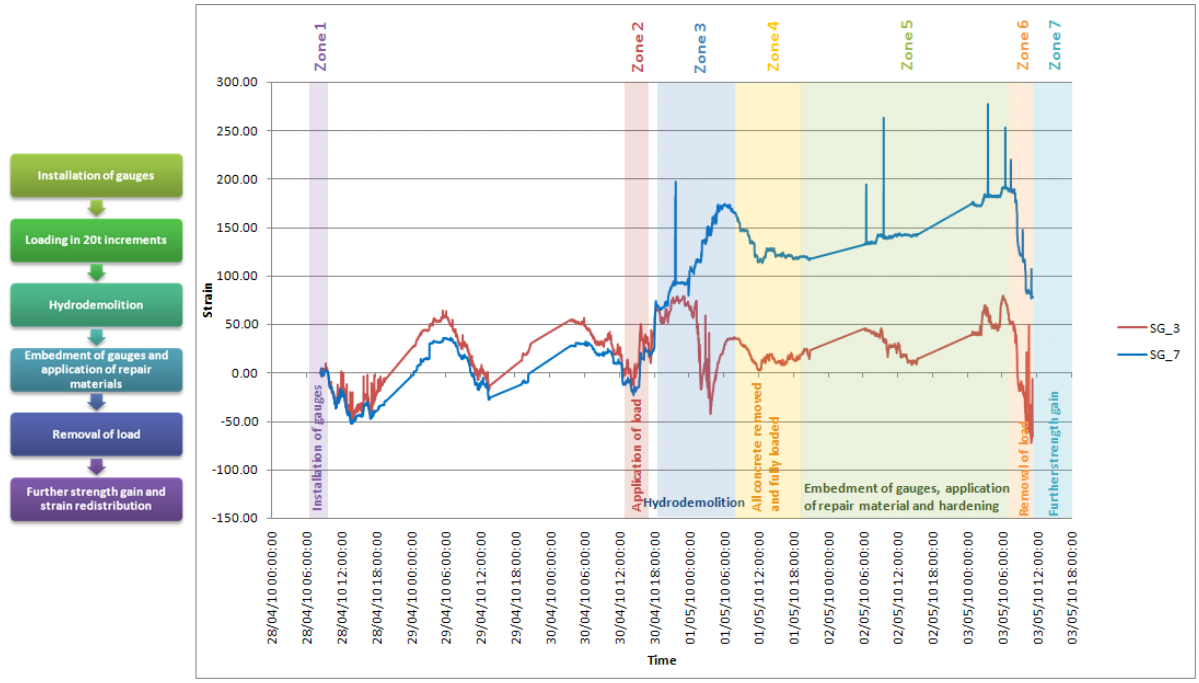


Figure 3. Strain data from continuous monitoring for two representative strain gauges on the bridge, with activities and time zones related to such activities identified.

Embedded strain gauges (SG 11, 12 and 13) were directly attached to the tendons before the hydrodemolition process and were zeroed at a later time than the other gauges and activities. Consequently, a direct comparison of the embedded gauges with the other gauges is not necessarily appropriate at all times. Also, these gauges are important since they are located at the centre of the damage and the responses to different activities in these gauges are often more stark than the gauges installed at the beginning. Additionally, the embedded gauges are the only gauges that are sheltered from thermal effects and are in direct contact with the hardening repair material. Table 1 provides the different time zones over which the rehabilitation was carried out.

| Time Zone | Description of Activity |
|---|---|
| 1 | Installation of gauges<br>(barring embedded gauges SG11, SG12, SG13). |
| 2 | Loading in 20t increments up to 120t equally<br>on either side of damage in a nearly static fashion. |
| 3 | Hydrodemolition for concrete removal at damaged location. |
| 4 | Installation of embedded gauges SG11, SG12, SG13 and<br>application of repair materials. |
| 5 | Removal of preload following hardening of repair materials. |
| 6 | Further strength gain and possible strain redistribution. |

Table 1. Description of time zones and activities in the rehabilitation process.

**3. Methodology**

A generalised Hurst exponent approach was considered in this paper following established research [41]. A brief overview is provided here for completeness. The *q*-order moments of the distribution of the increments of the $j^{th}$ strain gauge reading at $t^{th}$ time instant $\varepsilon_j(t)$ , with $t=\nu, 2\nu,...k\nu,...T$ is studied, where $T$ is the time period of observation and $\nu$ is the time

resolution of observation and *k* is an arbitrary positive integer value. The stochastic evolution of $\varepsilon_j(t)$ is characterised and related to the generalised Hurst exponent *H*(*q*) through

$$K_q(\tau) = \frac{\left\langle |\varepsilon_j(t+\tau) - \varepsilon_j(t)|^q \right\rangle}{\left\langle |\varepsilon_j(t)|^q \right\rangle} \sim \left(\tau / \nu\right)^{qH(q)} \quad (1)$$

The paper typically considers the value of *q* as 1 and 2 at different circumstances to investigate the scaling. To investigate the variation of *H* with changing signal lengths over the entire time of monitoring, the lengths of the time series observations were varied. Additionally, a range of values of *q* were considered when investigating the scaling of *qH(q)* against *q* for different activity zones.

**4. Results**

The value of *H* was estimated for the entire timeline and for the identified time zones of varied activity for each strain gauge. Figure 4 presents the estimated Hurst exponents for *q*=1 and *q*=2 respectively for the entire period of monitoring for all of the gauges, as well as for each of the activity zones. The three-dimensional bar charts indicate exponents computed over the entire period of monitoring. These values form the basis of discussion of the nature of the Hurst exponent footprints due to different human activities. The figure also allows comparing the estimated Hurst exponents for some special cases, including exponents related to embedded gauges, damaged gauges and the relationship between top and bottom gauges. Spikes, jumps and sudden changes can significantly affect the estimation of Hurst exponent.

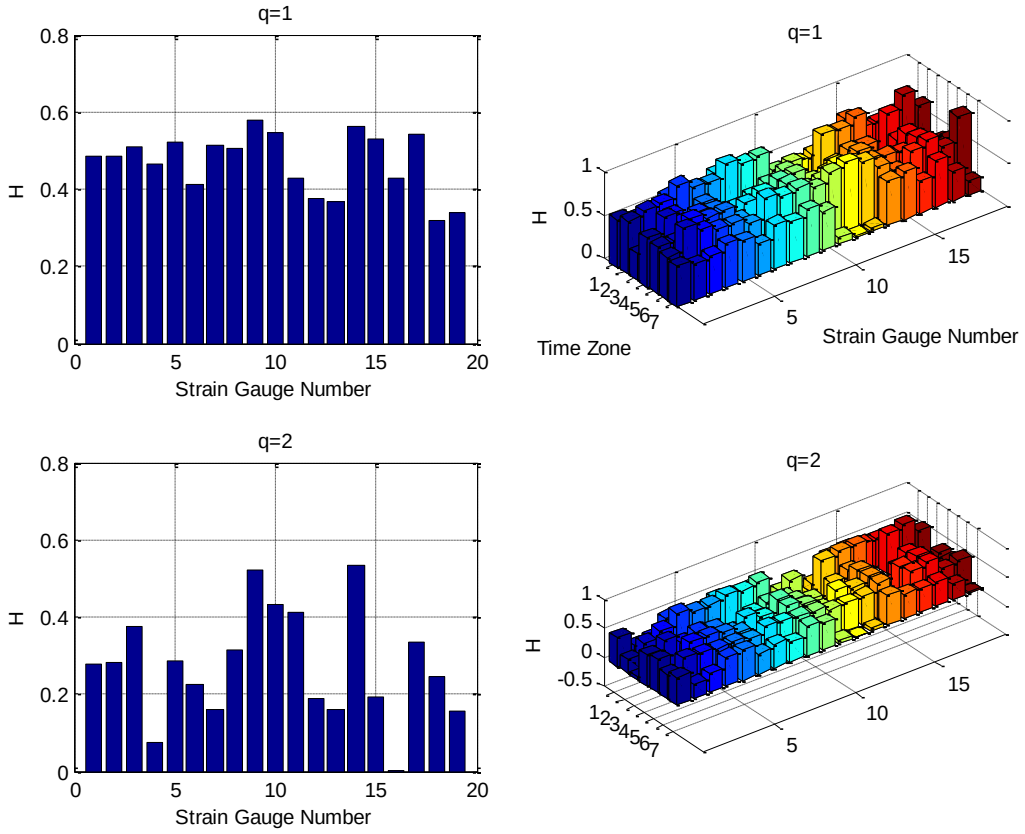


Figure 4. Estimated Hurst exponents computed for all gauges at different zones of activity.

Figure 4 reveals that the Hurst exponent footprint is extremely rich for this experiment, since the activity on the structure is significantly varied over time. Empirical studies on the estimated values can thus be of considerable interest. The estimation of exponents related to $q$=2 is more sensitive from gauge to gauge, while estimation related to $q$=1 tends to be more stable with gauges. Apart from the exponents computed over the entire time length, the variation of the exponents at different time zones is extremely significant. Varied activities are observed to have left unique Hurst footprints. In this connection, the values of embedded gauges are only relevant from the point in time at which they were installed within the location of damage. The Hurst footprints of damaged gauges warrant further investigation.

Also, it is important to note the presence of negative values of $H$ for $q$=2 indicating an alternating pattern in the plot.

Although the exponents related to top and bottom gauges do not represent any salient relationship, the average value of Hurst exponents at each Monitoring Point can be a representative marker of the activities at each location. This also provides a basis for comparing whether the response to the activities on the damaged beam is significantly different from the undamaged ones. The average estimated values of Hurst exponent, computed at each Monitoring Point (MP) and averaged over the strain gauges at the location of the point is compared in Figure 5 for all time zones. Damaged gauges were ignored during the averaging. Explicable variations of $H$, dependent on Monitoring Points are not apparent over the entire monitored time period. A low value at MP2 may suggest that the effect on activities at the location of damage is significant, but MP5 on an undamaged beam also produce a value of $H$ less than 0.5 for $q$=1. However, the computed Hurst exponents at different activity periods, or time zones, allow comparing very disparate activities quantitatively with respect to each other and rank them based on the effects of the activities. The exponent thus provides a measure to assess the effect of each activity on the structure.

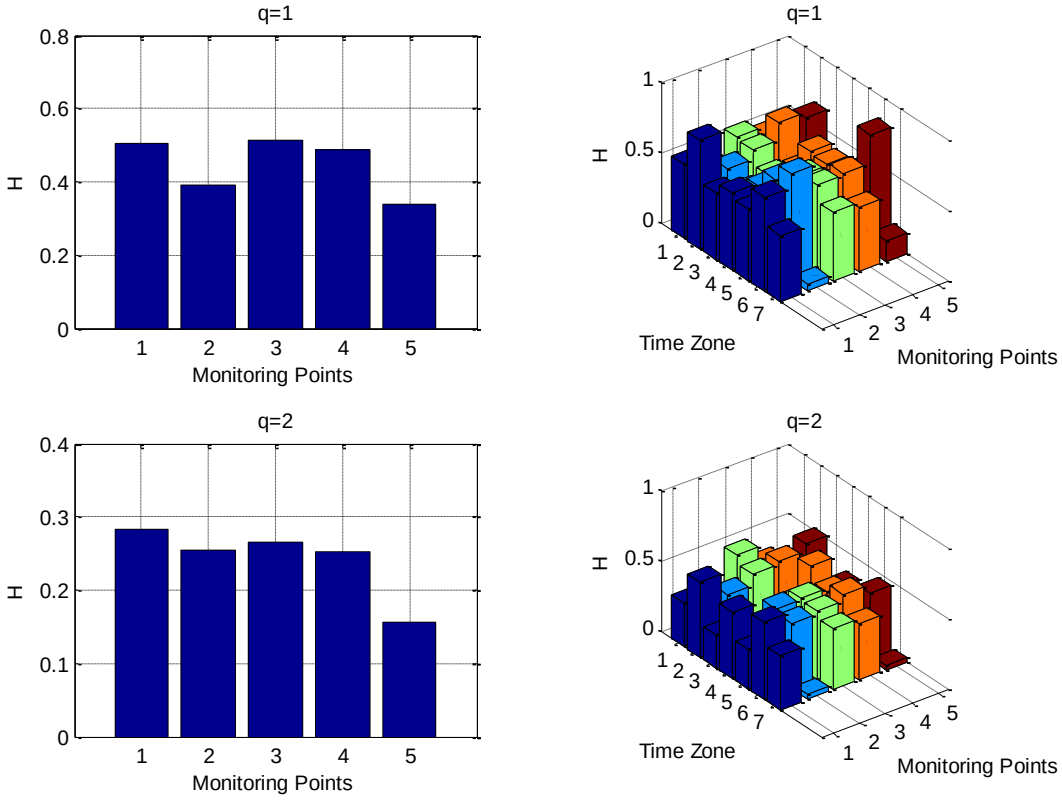


Figure 5. Estimated Hurst exponents computed for all Monitoring points for different activity.

Boxplots of estimated Hurst exponents are presented in Figure 6 to investigate the variations of this marker for different activities over time. The boxplots are presented by the gauges, as well as by the monitoring points. The eighth time zone on the horizontal axis corresponds to the entire monitoring period. The relative positioning of the different percentiles remain unchanged and form well-defined and relatively non-overlapped bunches for different activities. It is thus possible to relate the activities in terms of the computed exponents at different time zones of activity. A short discussion is provided next for results relating to $q$=1; similar conclusions may be drawn from $q$=2. During the relatively quiescent period of thermal action, the boxplot median is above 0.5, forming a base-case. The period of loading immediately after the thermal period consists of little change in temperature, a time zone during which the 120t load application is distributed equally over three loading events. There

is an uncertain, slow and relatively intermittent release of locked-in strains during this time as well. This period is characterised by a high *H* value. The hydrodemolition process is extremely dynamic and somewhat random by nature than the previous two time zones and this nature is reflected by a lowering of *H* during this activity. The consequent activity zones relating to gauge embedment, repair and hardening of repair materials and the removal of preload indicate an increasing quiescence and predictability in data series. However, this goes down once the preloads are removed and the structure is left to gain strength under diurnal thermal loading. The value of *H* during this second phase of thermal loading is lower than the first phase. The last columns in the graphs indicate the value of *H* for the entire monitoring period to provide the global benchmark of this value over the entire period of time and compare the various activities relative to it.

To understand how the values of *H* change locally, and how they relate to the computed exponents over the entire time period for each time zone, empirical investigations should be carried out on smaller data series windowed over the entire length of the signal. Estimating local values of *H* is a popular empirical marker for tracking jumps, changes or crashes in data although they may not necessarily be related to a certain theoretical paradigm. Nevertheless, these local values can provide an idea on what lengths of values, under what circumstances provide useful information that embodies the changes computed over the entire time lengths for each time zone of activity.

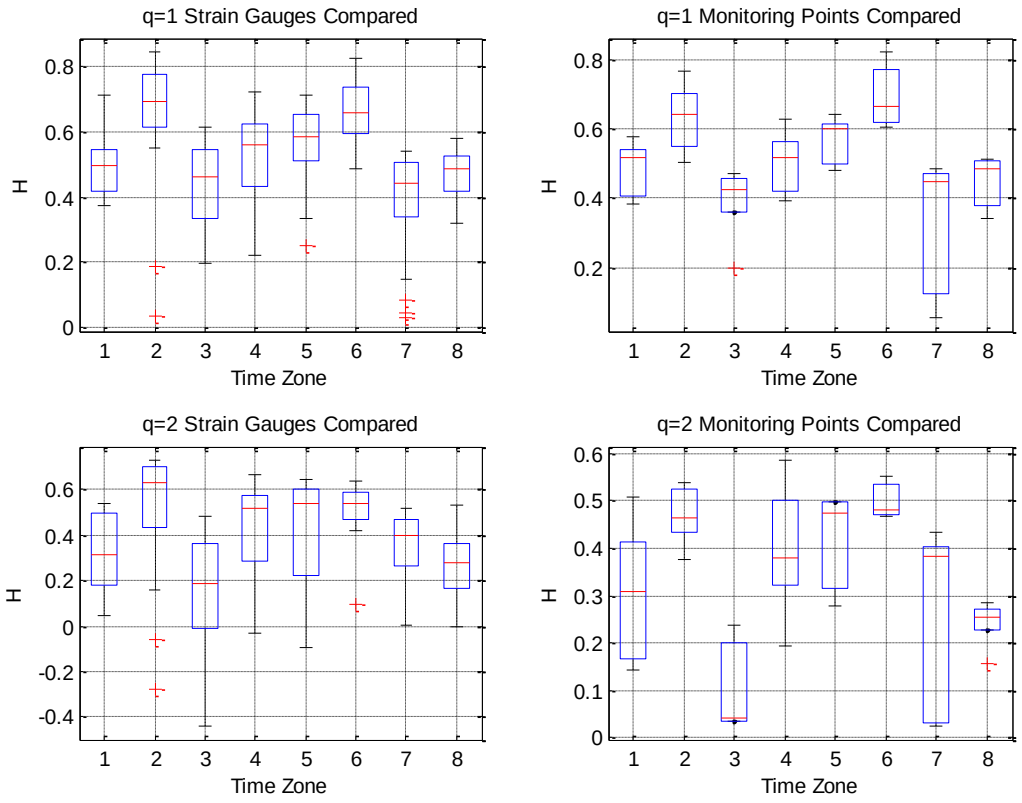


Figure 6. Boxplots of estimated Hurst exponents for different activities over time.

The behaviour of estimated local Hurst exponents computed over datasets of size significantly smaller than the original length of the dataset in investigated next. The variations of locally estimated exponents about the median, 25$^{th}$ percentile and 75$^{th}$ percentile values of the exponents computed over each time zone are studied. The lengths of windows considered for computing local exponents are 50 and 100 respectively. The two values correspond to the minimum value for which the computation of Hurst exponent is expected to be credible [41] and the minimum length of an entire time zone respectively. Figure 7 presents these variations of local Hurst exponent estimates. The comparisons with different percentiles are carried out by overlaying the average estimates in each event region, rescaled over the number of windows spanning the total length of the signal. The median, the upper quartile and the lower quartile are obvious from the positions on the overlaid graphs.

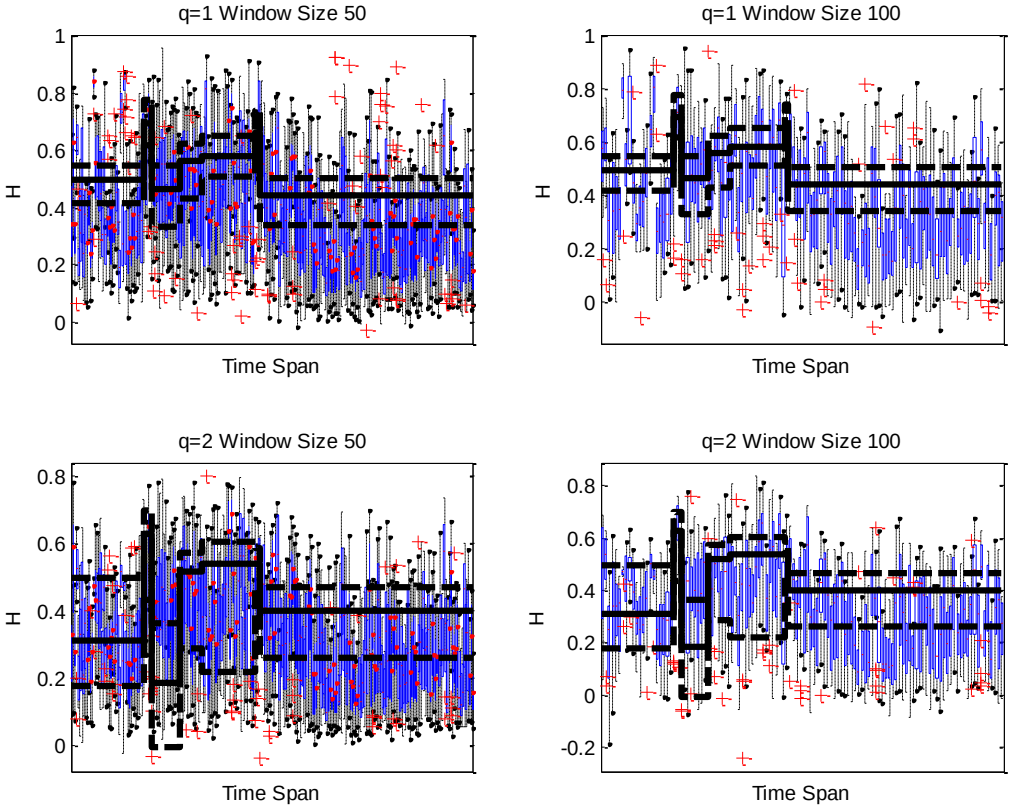


Figure 7. Boxplots of variations of local Hurst exponent estimates about the computed fractiles of Hurst exponents for each time zone.

It is observed that as the window size increases, the estimated local variation of *H* closely resembles the variations computed for the entire region of a time zone, representing a certain process of work. This is more pronounced for *q=2*, rather than for *q=1* but it is the size of the window that influences the reliable changes in events through locally estimated *H* and as compared to *H* estimated over an entire time zone. This method may only be used for monitoring when the governing activity is significantly larger in time than the minimum window size. Consequently, the locally estimated Hurst exponents may form a marker of health monitoring of structures, or identification of fundamental changes in activities.

Fundamental changes in activities or processes in various time zones can be viewed as relative deviations from pure Brownian models and to investigate the extent of multifractality

for different activities over the observed time zones, the scaling of *qH(q)* against *q* is investigated for different strain gauge locations through Figure 8. Additionally, Figure 9 and Figure 10 present similar scaling for damaged gauges and embedded gauges respectively.

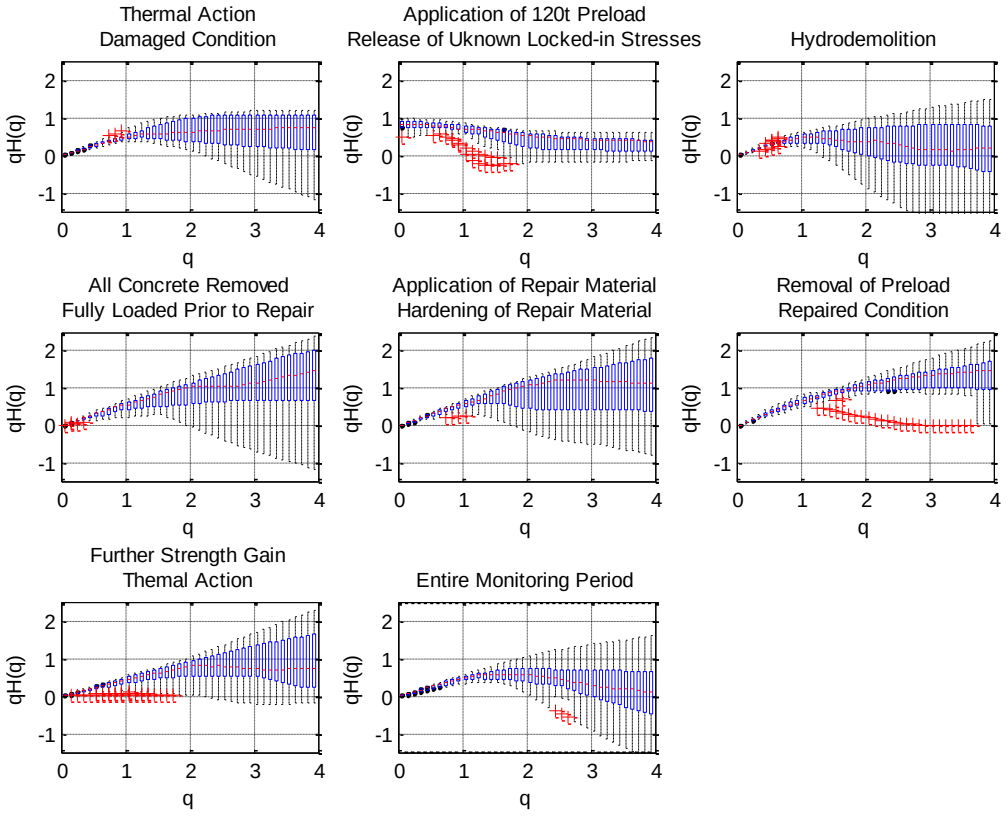


Figure 8. Boxplots of *qH(q)* versus *q* for different activities.

The boxplots of various activities in Figure 8 indicate that the processes may be characterised by *qH(q)* versus *q* boxplots, with each process showing evidences of multifractality existing in the system. The processes may be compared by the similarity of evolution of the *qH(q)* versus *q* boxplots. The most dissimilar time-series in this problem turns out to be the complex release of locked-in strain during the loading phase, although the hydrdodemolition period was by far the noisiest. The difference before and after the monitoring phase during exposure to relatively quiescent thermal action indicate the fundamental changes in the response of the structure following repair works. Also, it is important to note the similarity in evolution of

*qH(q)* versus *q* and the small deviations despite the similarity of the quasi-static time zones related to fully loaded condition under complete removal of concrete, application of repair material with consequent hardening and removal of preload respectively. Additionally, the scaling of *qH(q)* versus *q* deviated very significantly from linearity for values of *q* greater than 2. Such evolutions of boxplots demonstrate a potential to quantify and compare very disparate processes with unknown models under output-only conditions.

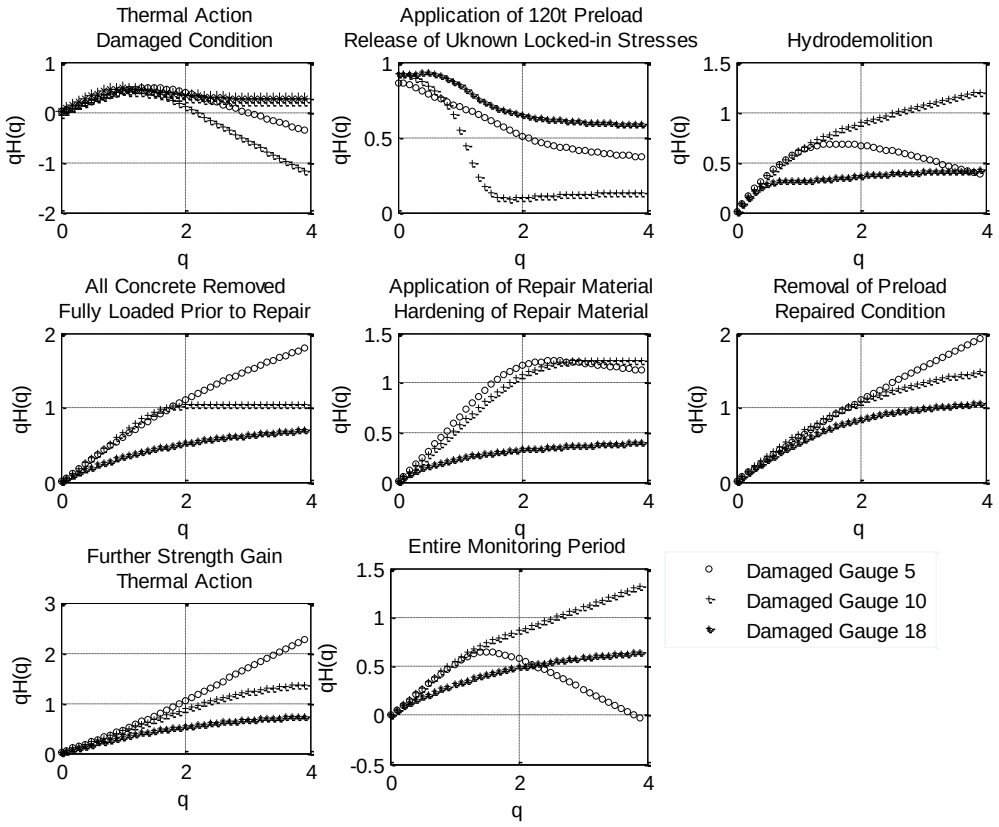


Figure 9. Plot of *qH(q)* versus *q* for different activities on damaged gauges.

The detection evolution of *qH(q)* versus *q* can thus be important for characterising the damaged gauge. The detection of a damaged gauge from significant deviation of the evolution of *qH(q)* versus *q* from the undamaged gauges would indicate fundamentally different processes being present in the gauges. However, not all the damaged gauges are affected in the same way. While some gauges are completely damaged and leave a Hurst

exponent evolution signature very different from the normal gauges and the related prevailing activities, there may also be gauges which are probably damaged due to poor connection with the structure or other conditions where they react to the prevailing activities, but the recorded values are not useful. The latter condition may be due to presence of high noise, variability or a sudden jump or change in baseline strain conditions.

Figure 9 indicates that the Hurst signature of activities may still be well-retained in damaged gauges depending on the type of activity. Gauges 5 and 10 correspond to a sudden change of baseline during the activities and then relatively poor response to the varying activities as compared to the other gauges. On the other hand gauge 18 corresponds to the sudden change and then continued recording of very high and noisy values against varied activities.

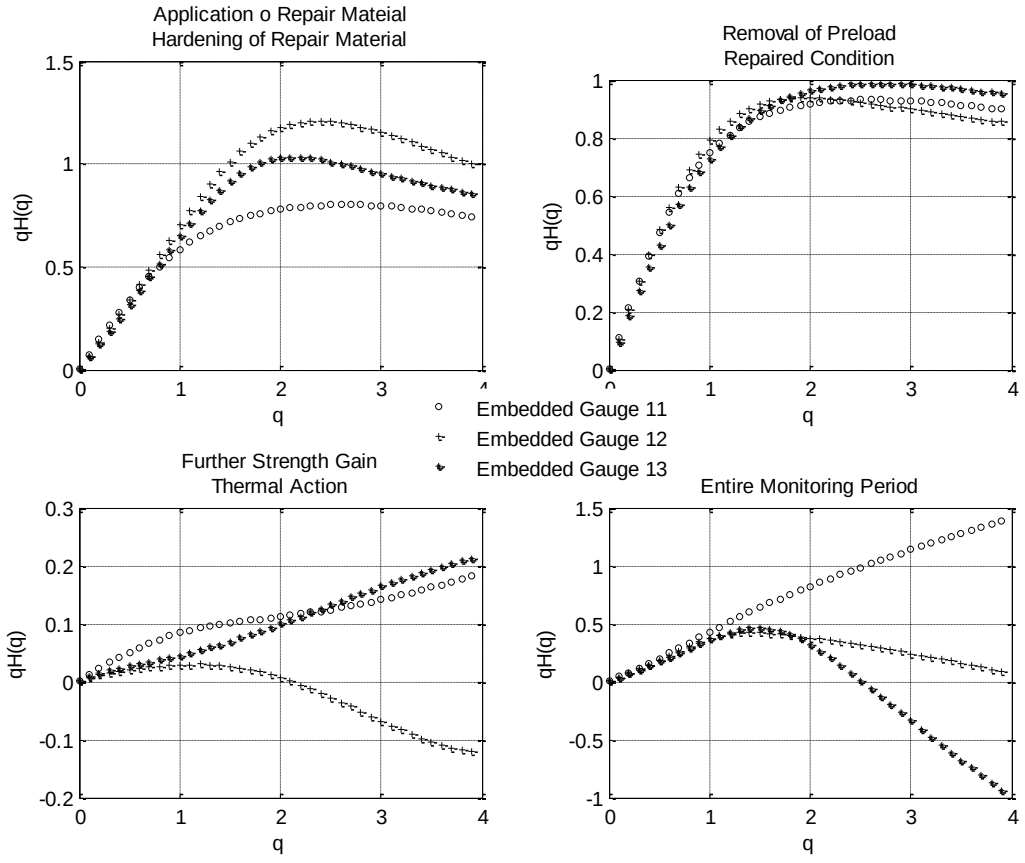


Figure 10. Plot of *qH(q)* versus *q* for different activities on embedded gauges.

The investigation of the embedded gauges indicate that the scaling of *qH(q)* versus *q* may not necessarily be extremely stable. The location is particularly affected by the activities carried out, but it also significantly exposed to the uncertainties and noise, bringing about significant changes among the *qH(q)* versus *q* plot. Consequently, rather than a gauge by gauge approach, the choice of a Monitoring Point, can be a good indicator, as has been shown in Figure 6. However, for activities particular to the location of the embedded gauges, the computed *qH(q)* versus *q* are very close, indicating the proximity of the gauges to the activity and the local nature of the activity itself. This is evident from Figure 10 where local action of repair material and the removal of preload under repaired condition result in close agreement of the graphs obtained from all three embedded gauges.

A measure of the degree of multifractality present in the signals is defined as the estimated width of the multifractal spectra [42,43]. The relative degrees of multifractality for different gauges in time zones of varied activity are presented in Figure 11. The maximum value of the degree of multifractality is presented by time zone 6, when the preloading is removed in three stages and the bridge tries to return to a repaired condition with perhaps some prestressing back into the system. Stress redistribution within the bridge structure may be responsible for this higher degree of multifractality. The embedded gauges react significantly to the zone of hydrodemolition, an activity to which they are exposed to the maximum. The monitoring points are comparable to each other.

An investigation into the source of multifractality was carried out next to assess whether the observations are due to long-range dependence or fat tailed distribution. The shuffled strain gauge readings were considered in this regard and the scaling of *qH(q)* versus *q* were plotted for each time zone of activity (Figure 12).

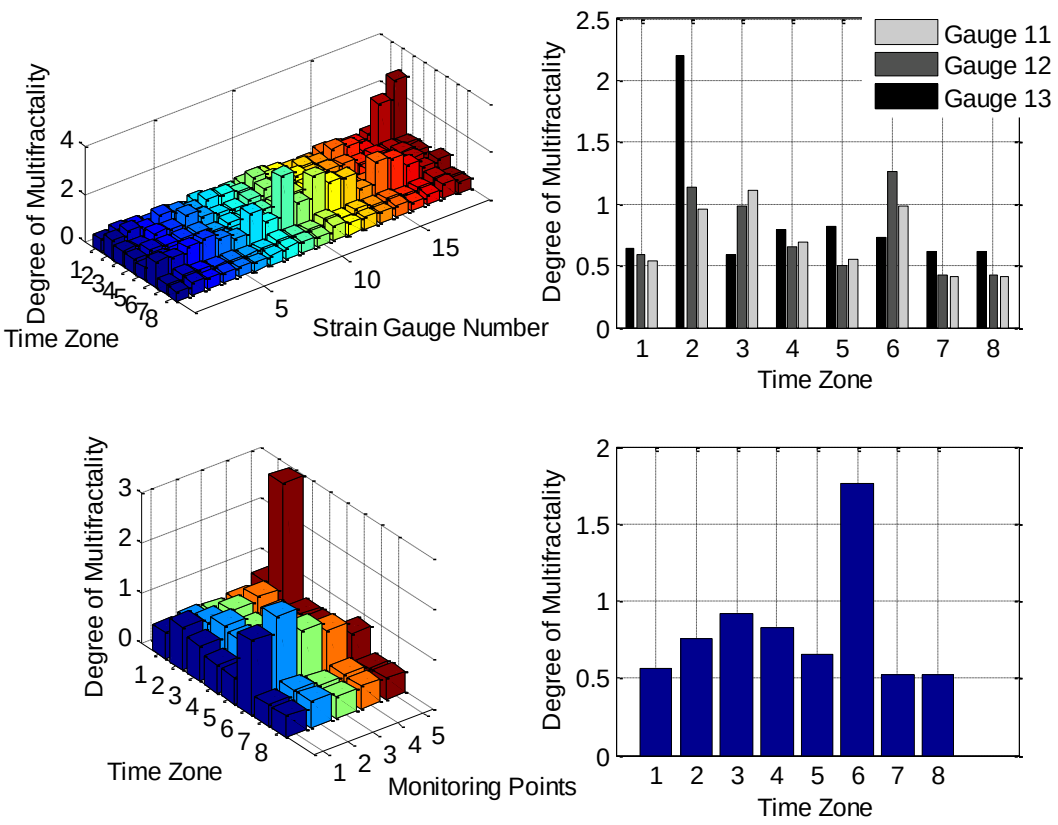


Figure 11. Estimated relative degrees of multifractality of different gauges at different time zones.

The idea is to destroy the correlation structure but preserve the distribution on the data. The shuffling is carried out by randomly permuting the location of the data points within the time series. It is observed that the scaling obtained from the original data is substantially changed after shuffling. However, a perfectly non-multifractal scaling is not evident either, suggesting that there may be some influence of distribution function. The estimated relative degrees of multifractality are estimated similar to Figure 11 and it is observed that the degree of multifractality is weaker for the shuffled series as compared to the original. The long range correlations is perhaps more dominant.

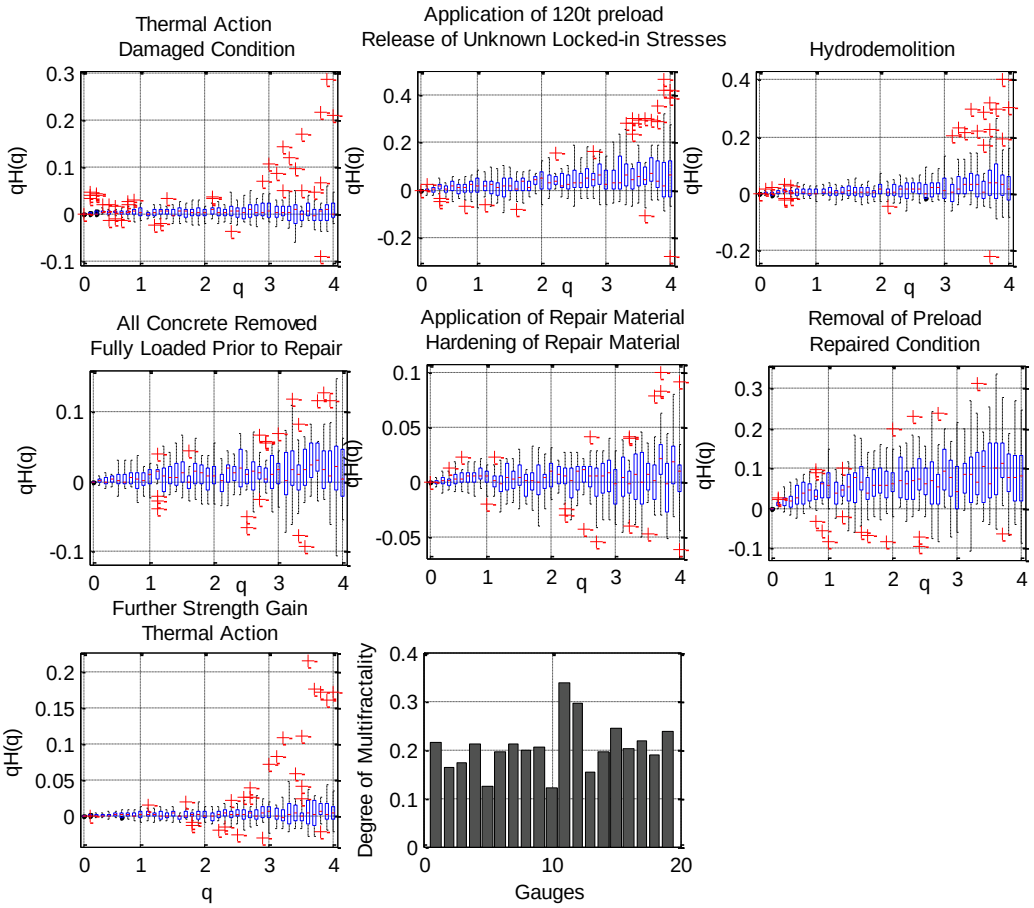


Figure 12. Boxplots of *qH(q)* versus *q* for different activities for shuffled time series and degrees of multifractality in shuffled time series data for different gauges.

The rolling window presented is Figure 7 can be an important monitoring measure even when the computed Hurst exponents may not have significant interpretation due to small number of values within the window (in the present example, 100 points captured the changing activities with less variation). However, to investigate how the degree of multifractality changes with time window, the entire monitoring period has been divided into dyadic fractions. The results are presented in Figure 13 for a healthy gauge, a damaged gauge and an embedded gauge. It is observed that the variation of degree of multifractality gradually increases with the dyadic scale of time division. With a small enough time window, it is possible to capture the degree of multifractality within each zone.

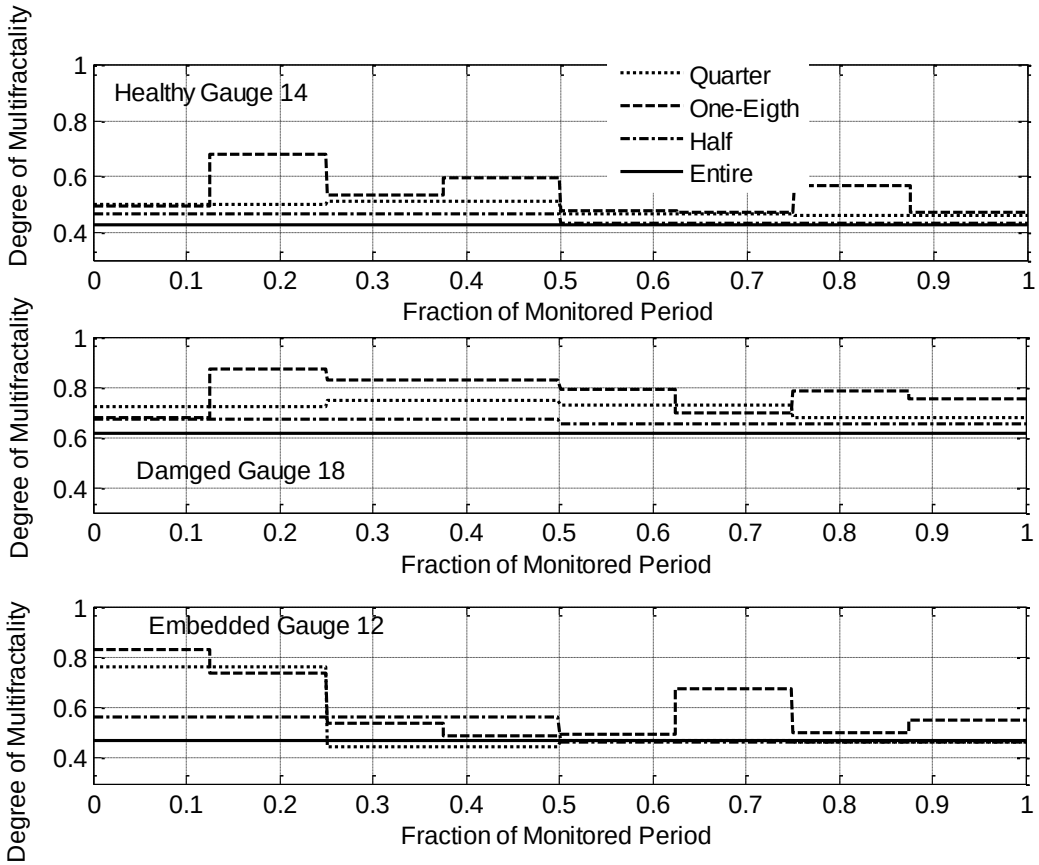


Figure 13. Time dependence of degree of multifractality for different gauges.

The second order difference moments [44] have been computed for the gauges over the time of monitoring. The Hurst exponent approach presented here has a better interpretation for high-frequency observations. However, the second order difference moments allow comparing the values for a range of time lags. The undamaged, damaged and the embedded gauges appear to bunch distinctly by their second order difference moments with respect to a very wide range of time lag (Figure 14). Of particular importance is the significant deviation of one of the gauges, which implies that of the three gauges damaged, two are of similar nature, while the third one has a different type of failure governing it. The observations from Figure 14 provide the basis for a number of studies for a future piece of work focusing on the quantification of different components of fluctuation and of nonlinearities. In particular, the observations provide the basis for assessing, from a purely output-only sparsely sampled

pseudo-dynamic data, the components related to system specific resonances and interferential contributions at lower frequencies [45]. For future studies, it would be interesting to investigate cross-correlations based on difference moments [46,47], including comparisons at different gauges of the same monitoring point. These studies, along with delay vector variance type approaches [48,49,50] will be important in terms of establishing validated guidelines of handling large infrastructure system responses from an output-only condition.

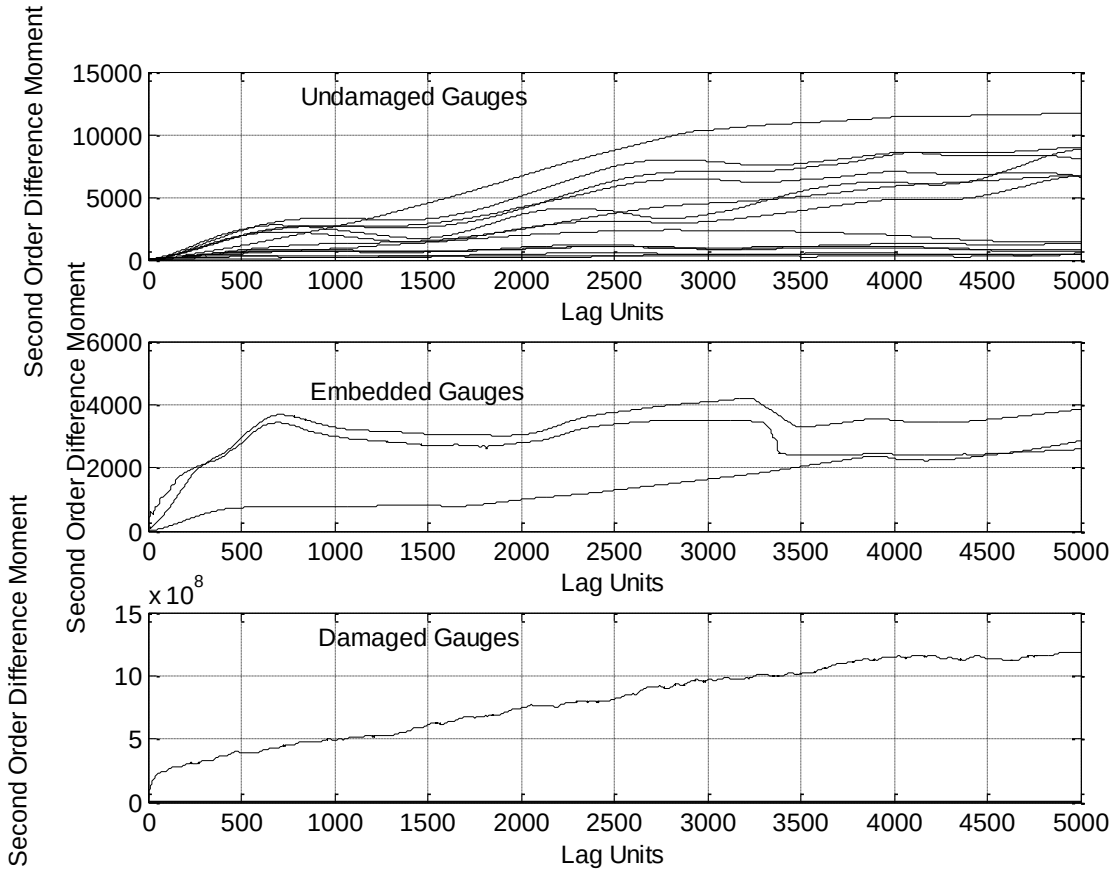


Figure 14. Second order difference moments compared for different gauges.

## 5. Conclusions

This paper presents the Hurst exponent footprints for very disparate human activities on a large structure in the form of full scale repair under continuous monitoring over the entire time period. Significant differences in Hurst exponents characterised significantly different

activities in different time domains. These observations were true for different strain gauges for monitoring, as well as different Monitoring Points where the exponents were averaged over a number of strain gauges. It is possible to track the changes of Hurst exponents for different activities by analysing relatively smaller lengths of data series and considering the boxplots of locally estimated Hurst exponents over time. However, the applications of such a method is dependent on the context of the application, as interpreted against the minimum time length required to credibly capture the computed exponent over each time zone corresponding to a particular activity. The evolution of boxplots of $qH(q)$ versus $q$ may be used as a marker to compare the relative similarities of different activities on large structures, and the relative deviation of the scaling from linearity may be used as a marker to quantify the complexity of the effect of each activity when a model is not available or is too difficult to be developed. Consequently, even in the absence of benchmarking, the Hurst exponent can provide certain insights to the activities on the system from output-only conditions. Even when it is visually not apparent, the damaged gauges may retain the Hurst footprints of various activities. Spatially local activities result in a relatively small deviation of Hurst exponent evolution at various scales for gauges close to such activities. However, there is no guarantee that spatially close gauges will result in closely spaced Hurst footprints for different activities. The degree of multifractality present was investigated at different time zones, involving all of the gauges. The source of multifractality was investigated through the analysis of shuffled series and the shuffled series exhibited a lower degree of multifractality as compared with the original system. The time dependence of the degree of multifractality was demonstrated on undamaged, damaged and embedded gauges. The computation of second order difference moments indicated the bunching of undamaged, damaged and embedded gauges separately. Specific directions of future work evolving from this study

were identified in the field of health monitoring of structures over a long period of time or during a rehabilitation process.

Empirical investigations involving the evolution of local or time averaged Hurst exponents or estimated degrees of multifractality at different spatial locations is observed to be a powerful tool for gaining insight into the nature of the complex processes affecting large structures with uncertain and varied exposure to activities. Additionally, this evolution allows comparing varied activities under a complete model-free, output based approach. Since a lot of these activities are related to the rehabilitation of structures, the approach can be used for monitoring activities and ensuring comparability among disparate activities. With further experiments, the current scarcity or absence in reporting such full scale monitoring in the light of empirical investigations through estimated Hurst exponents may be overcome and the varied activities may be standardised through this approach.

**Acknowledgements:**

The authors gratefully acknowledge the involvement and help of the following:

*The National Roads Authority, Maudlins, Naas, Kildare, Ireland*

*South Dublin County Council, Tallaght, Dublin, Ireland*

*Coastway, Naas, Kildare, Ireland*

*Datum Monitoring Services Limited, Moira, Armagh, Northern Ireland*

*Structural Concrete Bonding Services Limited, Newbridge, Kildare, Ireland*

*Complete Highway Maintenance Group, Walkinstown, Dublin, Ireland*

*Testconsult Ireland Limited, Portlaoise, Laoise, Ireland*

## Reference


[1] P. Nourozzadeh, G.R. Jafari. Application of multifractal measures to Tehran price index, Physica A, 356 (2005) 609 – 627.

[2] R. Weron, B. Przybyłowicz. Hurst analysis of electricity price dynamics, Physica A, 283(3-4) (2000) 462 – 468.

[3] J. Peng, Z. Liu, J. Wu, Y. Han. Trend analysis of vegetation dynamics in Qinghai-Tibet plateau using Hurst exponent, Ecological Indicators, 14(1) (2012) 28 – 39.

[4] T. Costa, D. Galati, E. Rognoni. The Hurst exponent of cardiac response to positive and negative emotional film stimuli using wavelet, Automatic Neuroscience, 151(2-3) (2009) 183 – 185.

[5] M. Li. Change trend of averaged Hurst parameter of traffic under DDOS flood attacks, Computers & Security, 25(3) (2006) 213 – 220.

[6] D.O. Cajueiro, B.M. Tabak. Is the expression H=1/(3-q) valid for real financial data?, Physica A, 373 (2007) 593 – 602.

[7] J. Mielniczuk, P.Wojdyłło. Estimation of Hurst exponent revisited, Computational Statistics & Data Analysis, 51 (2007) 4510 – 4525.

[8] F. Serinaldi. Use and misuse of some Hurst parameter estimators applied to stationary and non-stationary financial time series, Physica A, 389 (2010) 2770 – 2781.

[9] S. Katsev, I. L'Heureux. Are Hurst exponents estimated from short or irregular time series meaningful?, Computers & Geosciences, 29 (2003) 1085 - 1089

[10] M.J. Cannon, D.B. Percival, D.C. Caccia, G.M. Raymond, J.B. Bassingthwaighte. Evaluating scaled windowed variance methods for estimating the Hurst coefficient of time series, Physica A, 241 (1997) 606 – 626.

[11] J. Alvarez-Ramirez, J.C. Echeverria, E. Rodriguez. Performance of a high-dimensional R/S method for Hurst exponent estimation, Physica A, 387 (2008) 6452 – 6462.

[12] J. Barunik, L. Kristoufek. On Hurst exponent estimation under heavy-tailed distributions, Physica A, 389 (2010) 3844 – 3855.

[13] C. Elllis. The sampling properties of Hurst exponent estimates, Physica A, 375 (2007) 159 – 173.

[14] R. Liu, T. Di Matteo, T. Lux. True and apparent scaling: The proximity of the Markov – switiching multifractal model to long – range dependence, Physica A, 383(1) (2007) 35 – 42.

[15] S. Kumar, N. Deo. Multifractal properties of the Indian financial market, Physica A, 388 (2009) 1593 – 1602.

[16] J. Alvarez-Ramirez, J. Alvarez, E. Rodriguez, G. Fernandez-Anaya. Time-varying Hurst exponent for US stock markets, Physica A, 387 (2008) 6159 – 6169.

[17] J. Alvarez-Ramirez, M. Cisneros, C. Ibarra-Valdez, A. Soriano. Multifractal Hurst analysis of crude oil prices, Physica A, 313 (2002) 651 – 670.

[18] M.S. Movahed, E. Hermanis. Fractal analysis of river flow fluctuations, Physica A 387 (2008), 915 – 932.

[19] C.C. Chen, Y.T. Lee, Y.F. Chang. A relationship between Hurst exponents of slip and waiting time data of earthquakes, Physica A, 387(18), 4643-4648.

[20] S. Rehman. Study of Saudi Arabian climatic conditions using Hurst exponent and climatic predictability index, Chaos Solitons & Fractals, 39 (2009) 499 – 509.

[21] C. Eom, S. Choi, G. Oh, W.S. Jung. Hurst exponent and prediction based on weak-form efficient market hypothesis of stock markets, Physica A, 387 (2008) 4630 – 4636.

[22] D. Grech, Z. Mazur. Can one make any crash prediction in finance using the local Hurst exponent idea?, Physica A, 336 (2004) 133 – 145.

[23] D. Grech, G. Pamuła. The local Hurst exponent of the financial time series in the vicinity of crashes on the Polish stock exchange market, Physica A, 387 (2008) 4299 – 4308.

[24] R. Morales, T. Di Matteo, R. Gramatica, T. Aste. Dynamical generalized Hurst exponent as a tool to monitor unstable periods in financial time series, Physica A, 391 (2012) 3180 – 3189.

[25] J. Alvarez-Ramirez, J.C. Echeverria, E. Rodriguez. Is the North Atlantic Oscillation modulated by solar and lunar cycles? Some evidences from Hurst autocorrelation analysis. Advances in Space Research, 47 (2011) 748 – 756.

[26] P.B. DePetrillo, d'A. Speers, U.E. Ruttimann, Determining the Hurst exponent of Fractal time series and its application to electrocardiographic analysis, Computers in Biology and Medicine, 29 (1999) 393 – 406.

[27] L.Y He, S.P Chen. Nonlinear bivariate dependency of price-volume relationships in agricultural commodity futures markets: A perspective from multifractal detrended crosss-correlation analysis, Physica A, 390 (2011) 297 – 308.

[28] H. Melhem, H. Kim. Damage Detection in Concrete by Fourier and Wavelet analyses, ASCE Journal of Engineering Mechanics, 129(5) (2003) 571-577.

[29] S. Nagarajaiah, N. Varadarajan. Short time Fourier transform algorithm for wind response control of buildings with variable stiffness TMD, Engineering Structures, 27 (2005) 431-441.

[30] D.Y Zheng, S.C Fan. Natural frequency changes of a cracked Timoshenko beam by modified Fourier Series, Journal of Sound and Vibration, 246(2) (2001) 297-317.

[31] P. Moyo, J.M.W Brownjohn. Detection of Anomalous Structural Behaviour using Wavelet Analysis, Mechanical Systems and Signal Processing, 16(2-3) (2002) 429-445.

[32] V. Pakrashi, B. Ghosh. Application of S transform in structural health monitoring, Non-Destructive Testing in Civil Engineering NDTCE09, 2009, Nantes, France.

[33] M.M. Reda Taha, A. Noureldin, J.L. Lucero, T.J. Baca. Wavelet transform for structural health monitoring: A Compendium of uses and features, Structural Health Monitoring, 5(3) (2006) 267-295.

[34] J. Arrigan, J, V. Pakrashi, B. Basu, S. Nagarajaiyah. Control of Flapwise Vibrations in Wind Turbine Blades using Semiactive Tuned Mass Dampers, Structural Control and Health Monitoring, 18(8) (2011) 840-851.

[35] V. Pakrashi, A. O'Connor, B. Basu. A Bridge-Vehicle Interaction Based Experimental Investigation of Damage Evolution, Structural Health Monitoring, 9(4) (2010) 285-296.

[36] R. Yan, R.X. Gao. Hilbert-Huang transform-based vibration signal analysis for machine health monitoring, IEEE Transactions on Instrumentation and Measurement, 55(6) (2006) 2320-2329.

[37] J. Trzasko, A. Manduca. Relaxed conditions for sparse signal recovery with general concave priors, IEEE Transactions on Signal Processing, 57(11) (2009) 4347-4354.

[38] Z. Xu, B. Huang, F. Zhang. Improvement of empirical mode decomposition under low sampling rate, Signal Processing, 89 (2009) 2296–2303.

[39] A. Aldroubi. Non-uniform weighted average sampling and reconstruction in shift-invariant and wavelet spaces, Applied Computational and Harmonic Analysis, 13 (2002) 151-161.

[40] A. Gentile, A. Messina A. On the Continuous Wavelet Transforms applied to discrete vibrational data for detecting open cracks in damaged beams. International Journal of Solids and Structures, 40 (2003) 295-315.

[41] T. Di Matteo, T. Aste, M.M. Dacorogna. Scaling behaviour in differently developed market, Physica A, 324 (2003) 183 – 188.

[42] J.W. Kantelhardt, E. Koscielny-Bunde, H.H.A Rego, S. Havlin, A. Bunde. Detecting long-range correlations with detrended fluctuation analysis, Physica A, 295 (2001) 441-454.

[43] E.A.F Ihlen, Introduction to multifractal detrended fluctuation analysis in Matlab, Frontiers in Physiology, 3(141) (2012) 1-18.

[44] S.F. Timashev, Y.S. Polyakov. Review of Flicker Spectroscopy in Electrochemistry, Fluctuation and Noise Letters, 7(2) 2007 R15-R47.

[45] R.M. Yulmetyev, S.A Demin, O.Yu. Panischev, P. Hänggi, S.F. Timashev, G.V. Vstovsky. Regular and stochastic behaviour of Parkinsonian pathological tremor signals. Phyica A, 369 (2006) 655-678.

[46] S.F. Timashev, Y.S. Polyakov, P.I. Misurkin, S.G. Lakeev. Anomalous diffusion as a stochastic component in the dynamics of complex processes. Physical Review E, 81(041128) (2010) 1-17.

[47] S.F. Timashev, O.Yu. Panischev, Y.S. Polyakov, S.A. Demin. Analysis of cross-correlations in electroencephalogram signals as an approach to proactive diagnosis of schizophrenia. Physica A, 391 (2012) 1179-1194.

[48] T. Gautama, D.P. Mandic, M.M. Van Hulle. The delay vector variance method for detecting determinism and nonlinearity in time series. Physica D, 190 (2004) 167-176.

[49] D.P. Mandic, M. Chen, T. Gautama, M.M. Van Hulle, A. Constantinides. On the characterization of the deterministic/stochastic and linear/nonlinear nature of time series. Proceedings of the Royal Society A, 464 (2008) 1141-1160.

[50] T. Gautama, D.P. Mandic, M.M. Van Hulle. Indications of nonlinear structures in brain electrical activity. Physical Review E, 67(046204) (2003) 1-5.

## LIST OF FIGURES

Figure 1

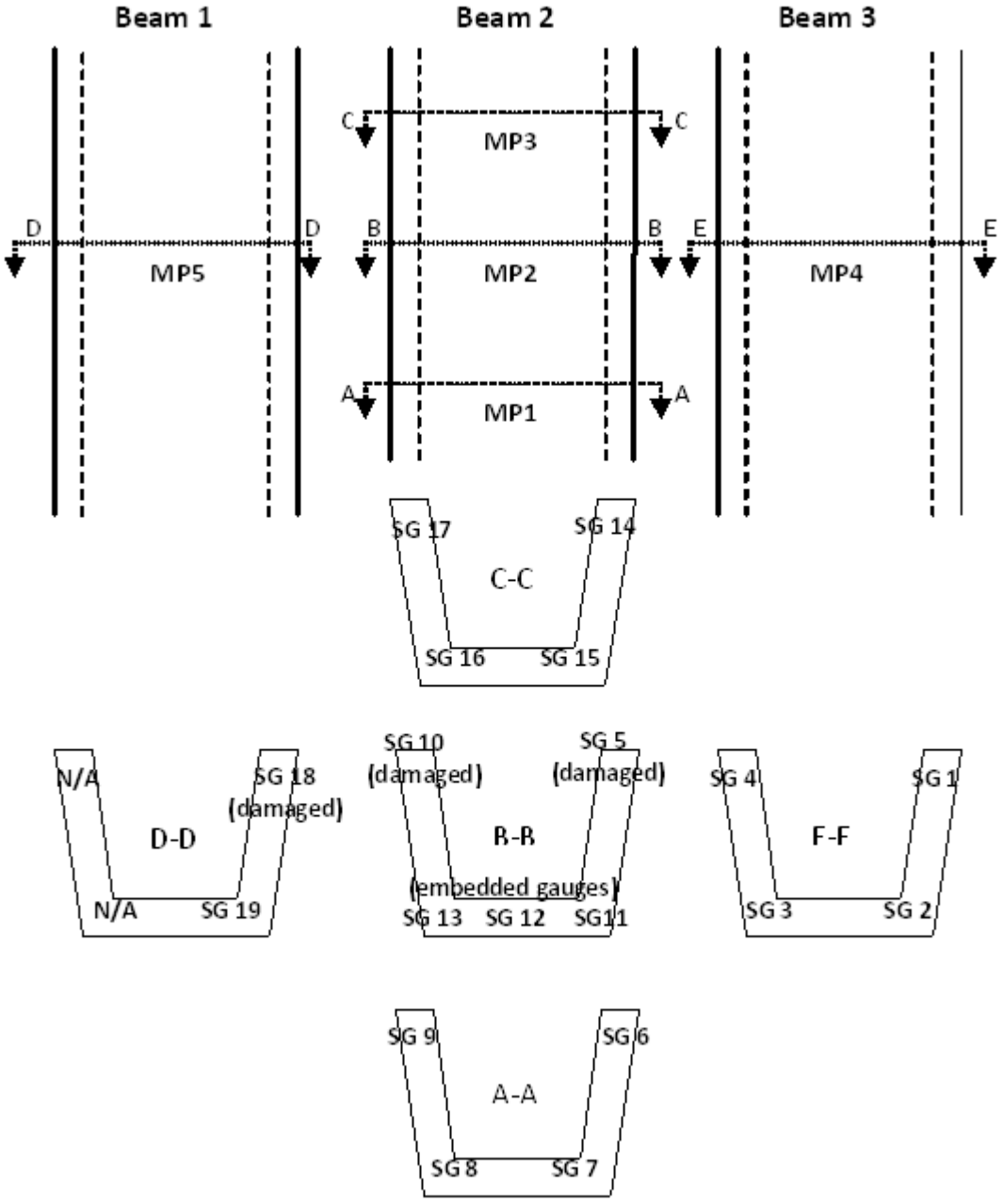
Beam 1
Beam 2
Beam 3
C
C
MP3
D
D
B
B
E
E
MP5
MP2
MP4
A
A
MP1
SG 17
SG 14
C-C
SG 16
SG 15
N/A
SG 18
(damaged)
D-D
N/A
SG 19
SG 10
(damaged)
SG 5
(damaged)
B-B
(embedded gauges)
SG 13
SG 12
SG11
SG 4
SG 1
F-F
SG 3
SG 2
SG 9
SG 6
A-A
SG 8
SG 7

Figure 2a

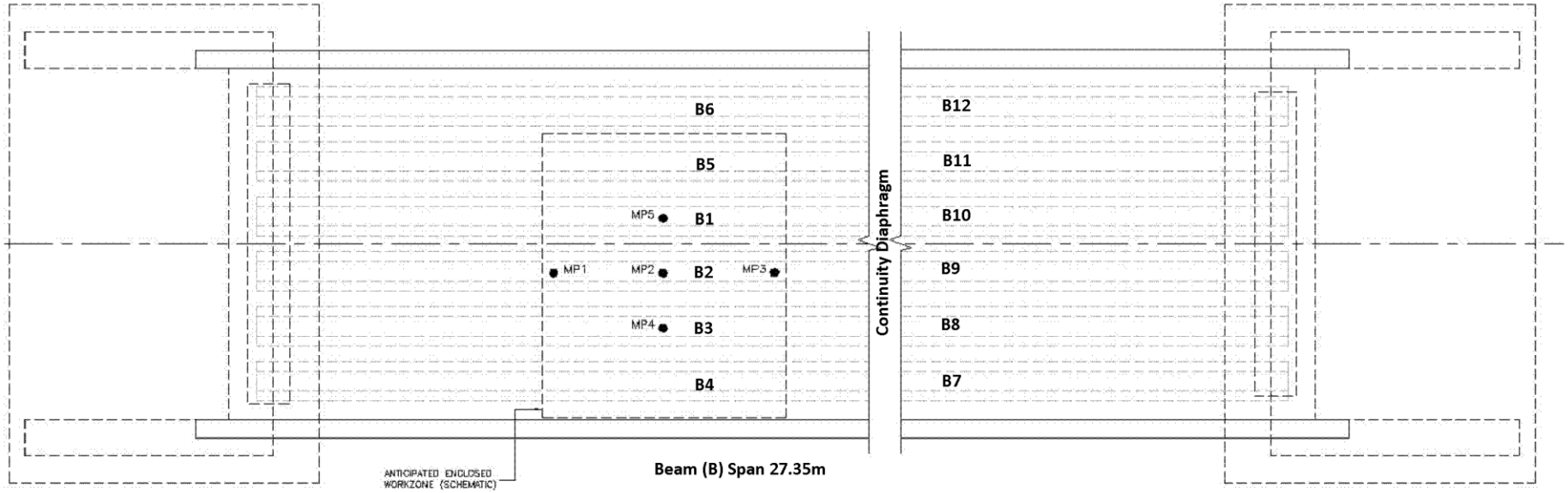
B6
B5
MP5
B1
MP1
MP2
B2
MP3
MP4
B3
B4
Continuity Diaphragm
B12
B11
B10
B9
B8
B7
ANTICIPATED ENCLOSED WORKZONE (SCHEMATIC)
Beam (B) Span 27.35m

Figure 2b

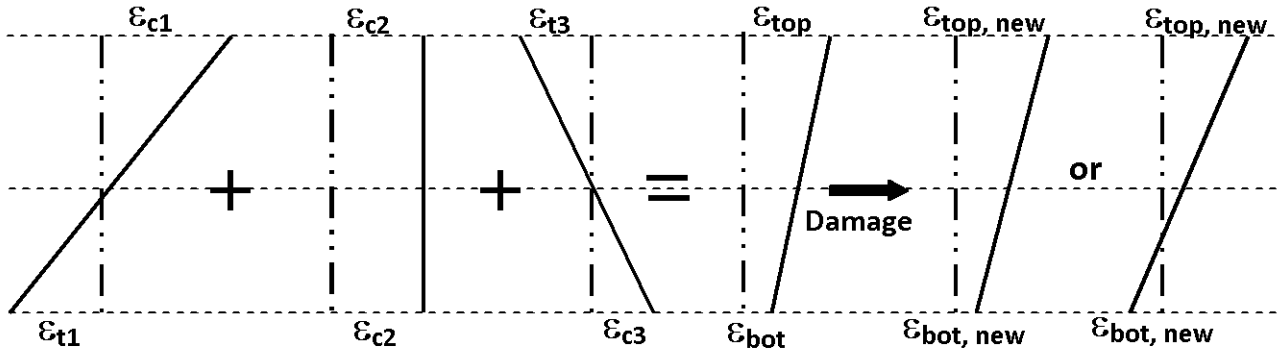
εc1
εc2
εt3
εtop
εtop, new
εtop, new
+
+
=
Damage
or
εt1
εc2
εc3
εbot
εbot, new
εbot, new

Figure 2c

Figure 2d

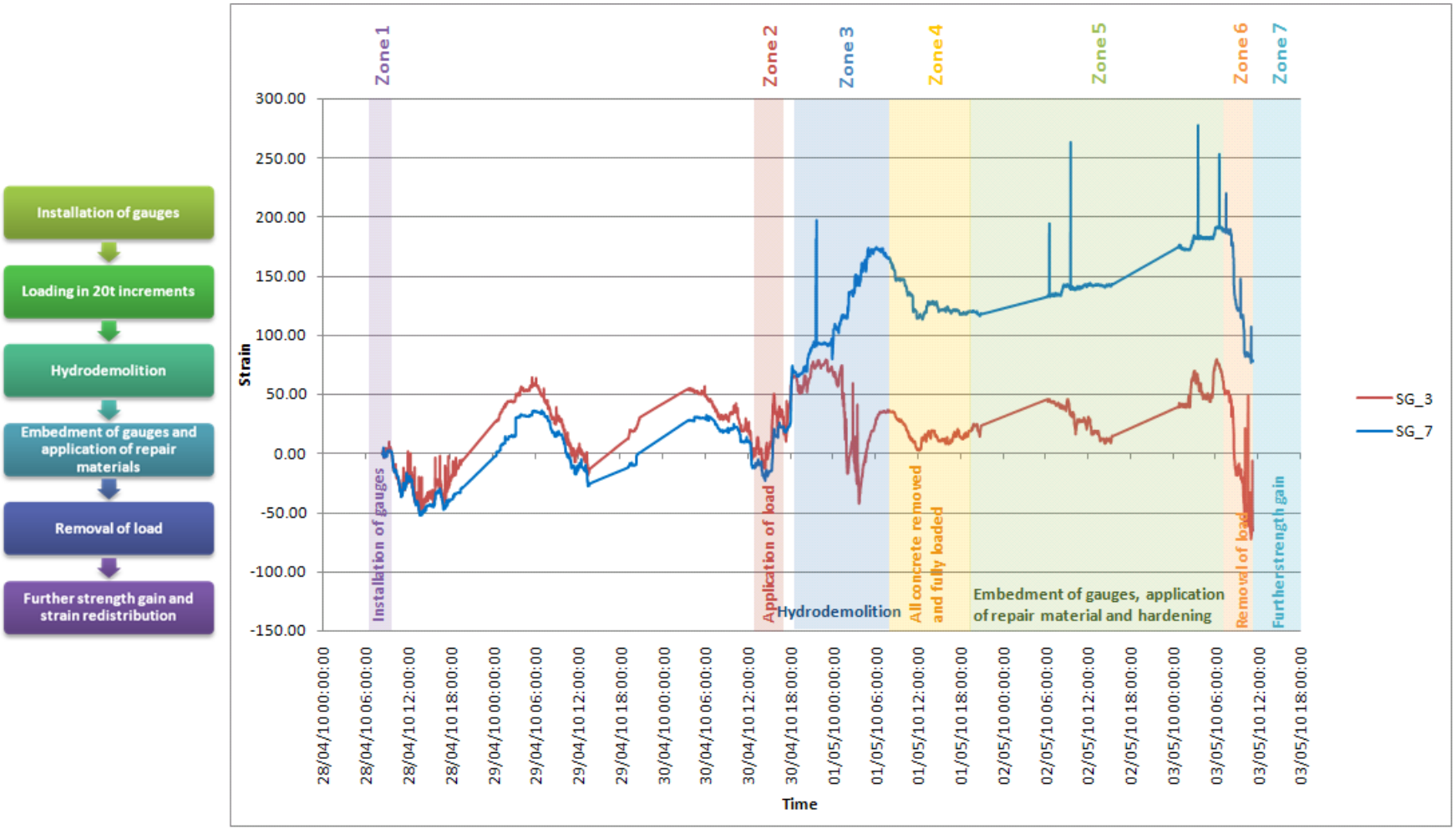
Installation of gauges
Loading in 20t increments
Hydrodemolition
Embedment of gauges and application of repair materials
Removal of load
Further strength gain and strain redistribution
Zone 1
Zone 2
Zone 3
Zone 4
Zone 5
Zone 6
Zone 7
Strain
300.00
250.00
200.00
150.00
100.00
50.00
0.00
-50.00
-100.00
-150.00
Installation of gauges
Application of load
Hydrodemolition
All concrete removed and fully loaded
Embedment of gauges, application of repair material and hardening
Removal of load
Further strength gain
28/04/10 00:00:00
28/04/10 06:00:00
28/04/10 12:00:00
28/04/10 18:00:00
29/04/10 00:00:00
29/04/10 06:00:00
29/04/10 12:00:00
29/04/10 18:00:00
30/04/10 00:00:00
30/04/10 06:00:00
30/04/10 12:00:00
30/04/10 18:00:00
01/05/10 00:00:00
01/05/10 06:00:00
01/05/10 12:00:00
01/05/10 18:00:00
02/05/10 00:00:00
02/05/10 06:00:00
02/05/10 12:00:00
02/05/10 18:00:00
03/05/10 00:00:00
03/05/10 06:00:00
03/05/10 12:00:00
03/05/10 18:00:00
Time
SG_3
SG_7

Figure 3

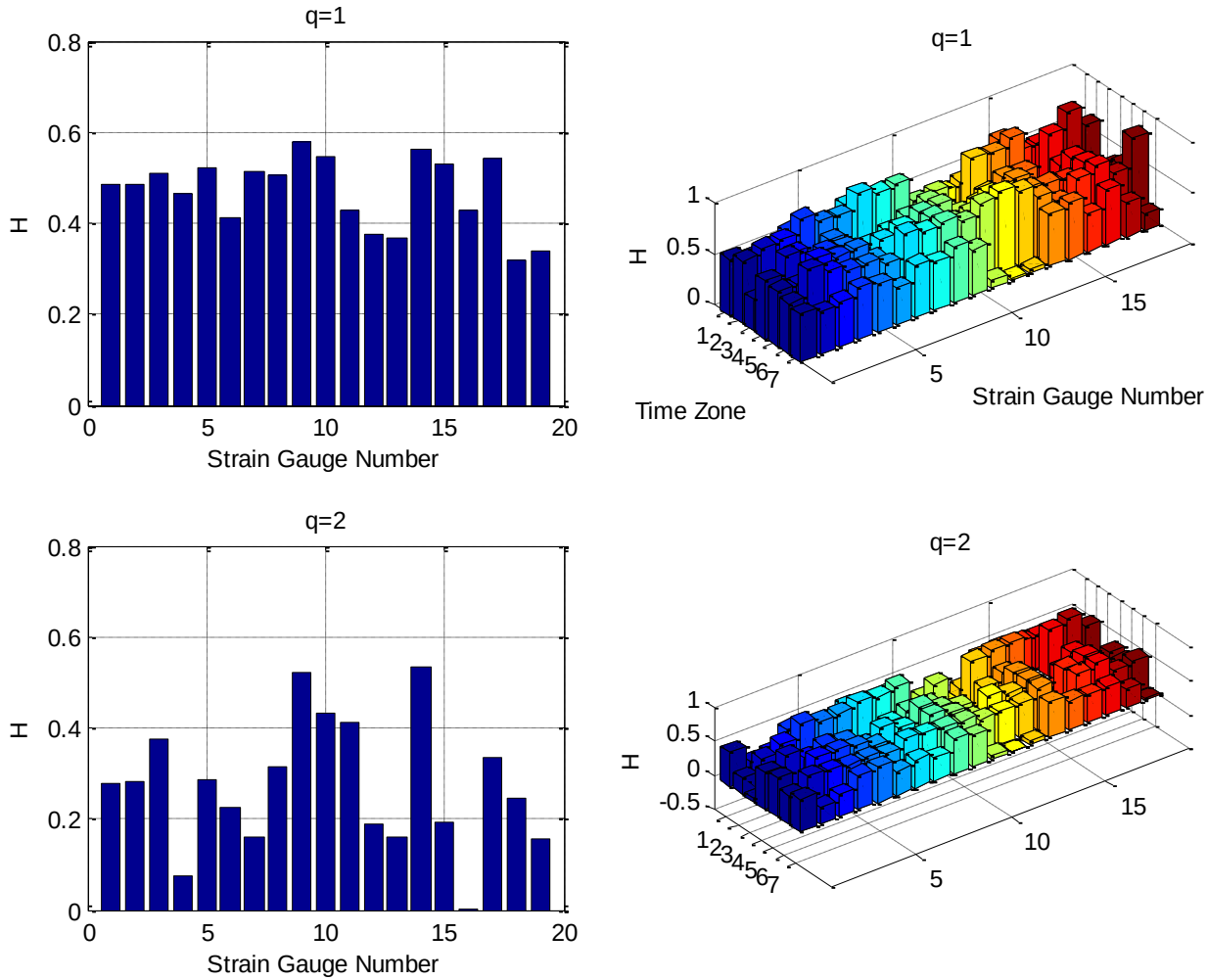
q=1
H
Strain Gauge Number
q=1
H
Time Zone
Strain Gauge Number
q=2
H
Strain Gauge Number
q=2
H

Figure 4

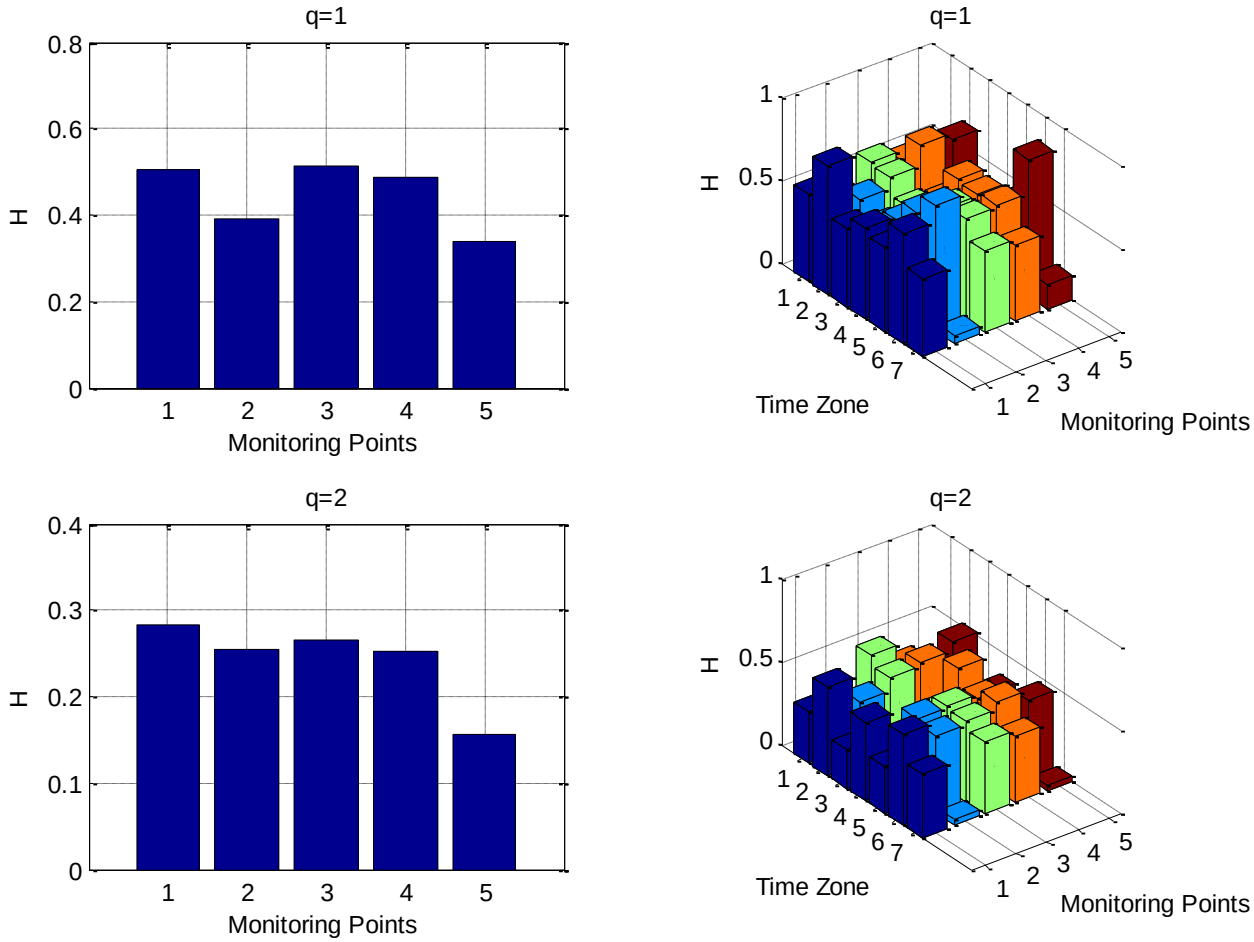


Figure 5

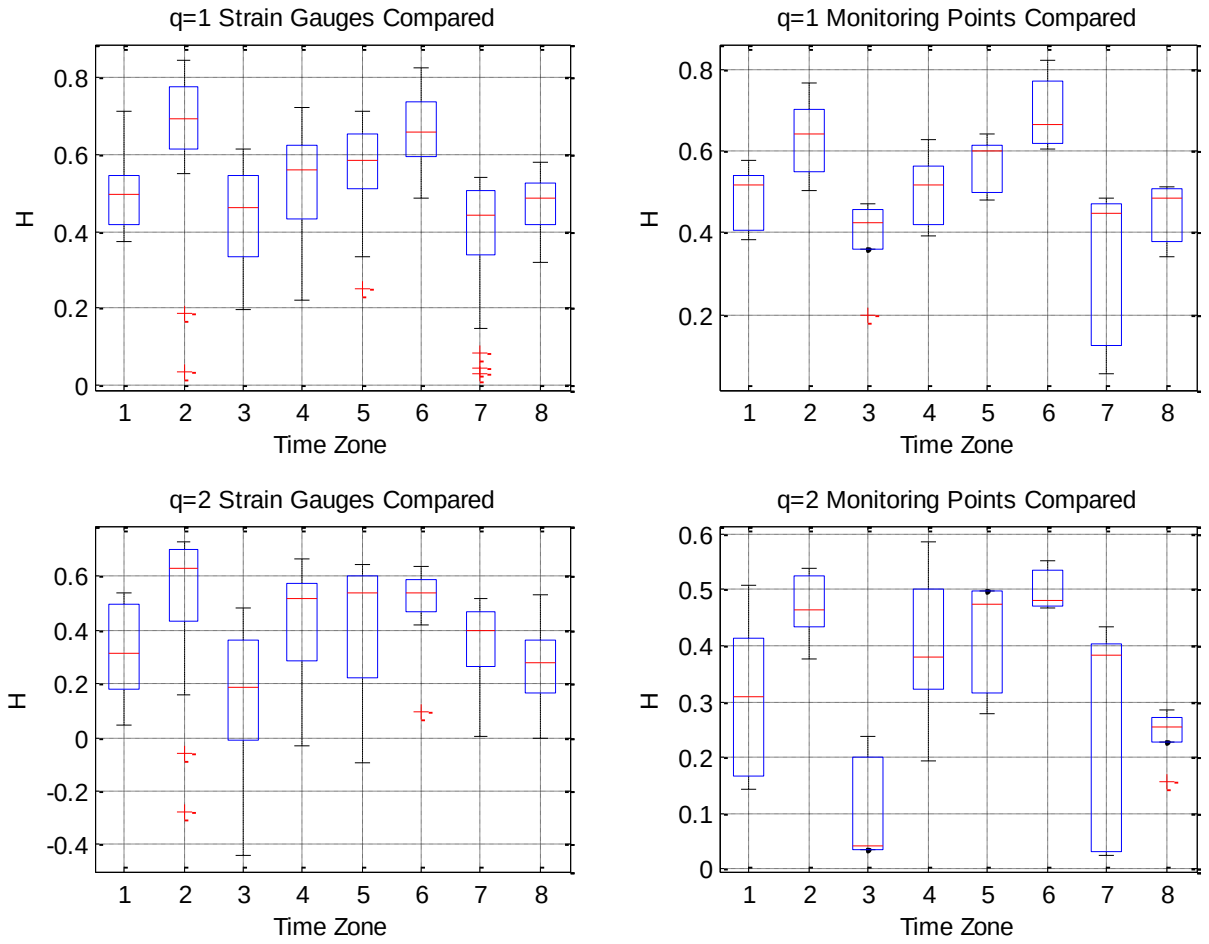
q=1 Strain Gauges Compared
H
Time Zone
q=1 Monitoring Points Compared
H
Time Zone
q=2 Strain Gauges Compared
H
Time Zone
q=2 Monitoring Points Compared
H
Time Zone

Figure 6

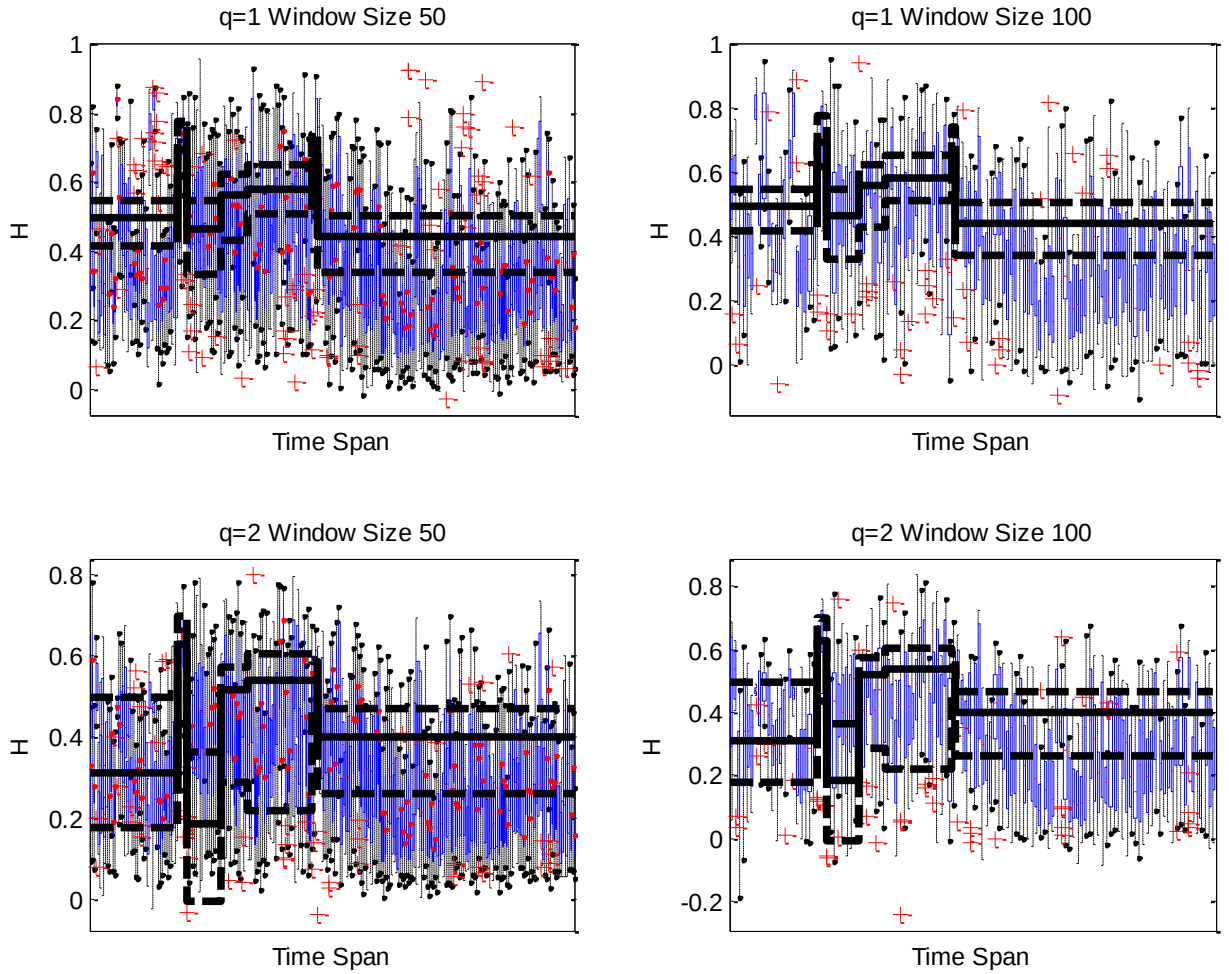
q=1 Window Size 50
H
Time Span
q=1 Window Size 100
H
Time Span
q=2 Window Size 50
H
Time Span
q=2 Window Size 100
H
Time Span

Figure 7

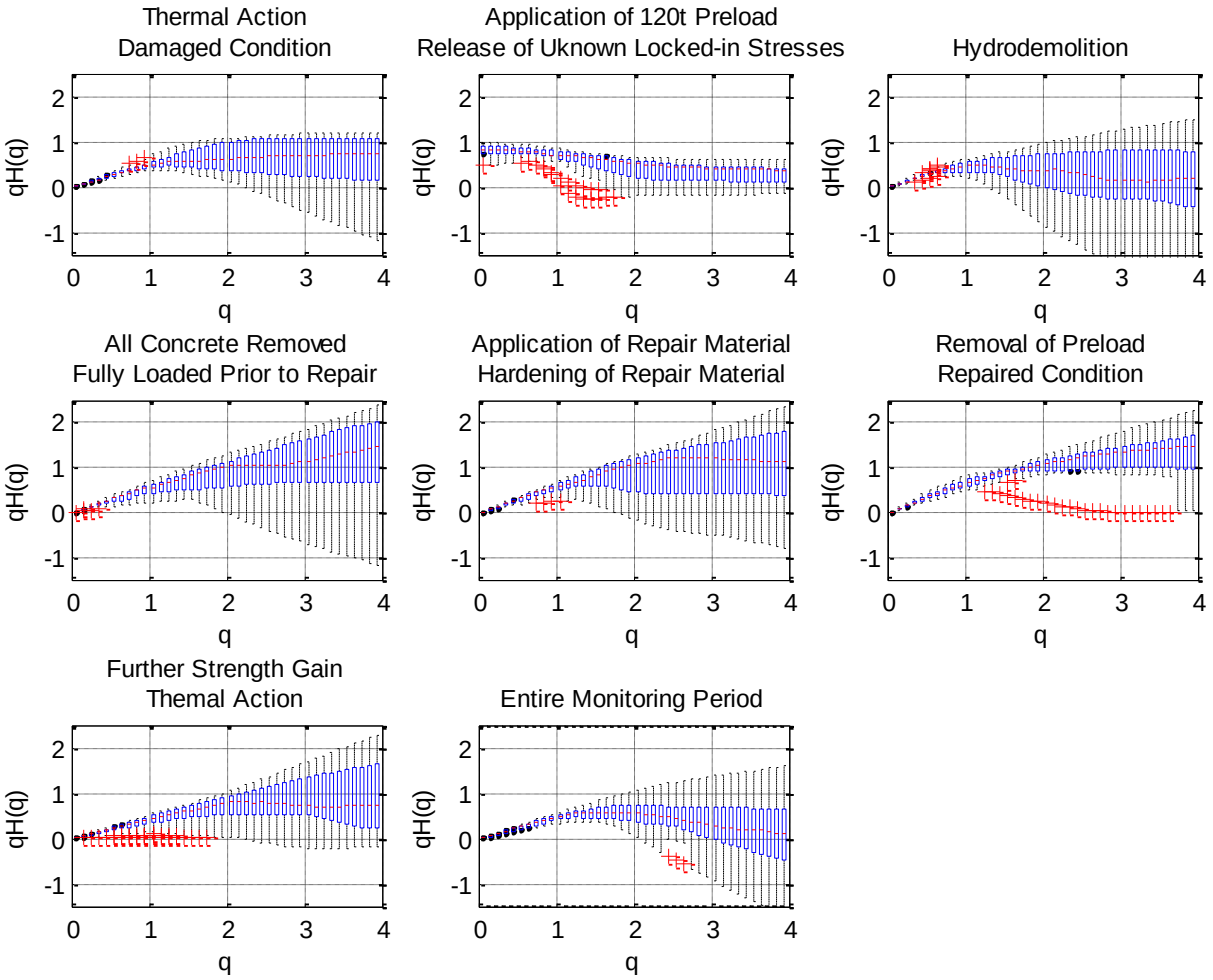
Thermal Action
Damaged Condition
Application of 120t Preload
Release of Uknown Locked-in Stresses
Hydrodemolition
All Concrete Removed
Fully Loaded Prior to Repair
Application of Repair Material
Hardening of Repair Material
Removal of Preload
Repaired Condition
Further Strength Gain
Themal Action
Entire Monitoring Period
qH(q)
q

Figure 8

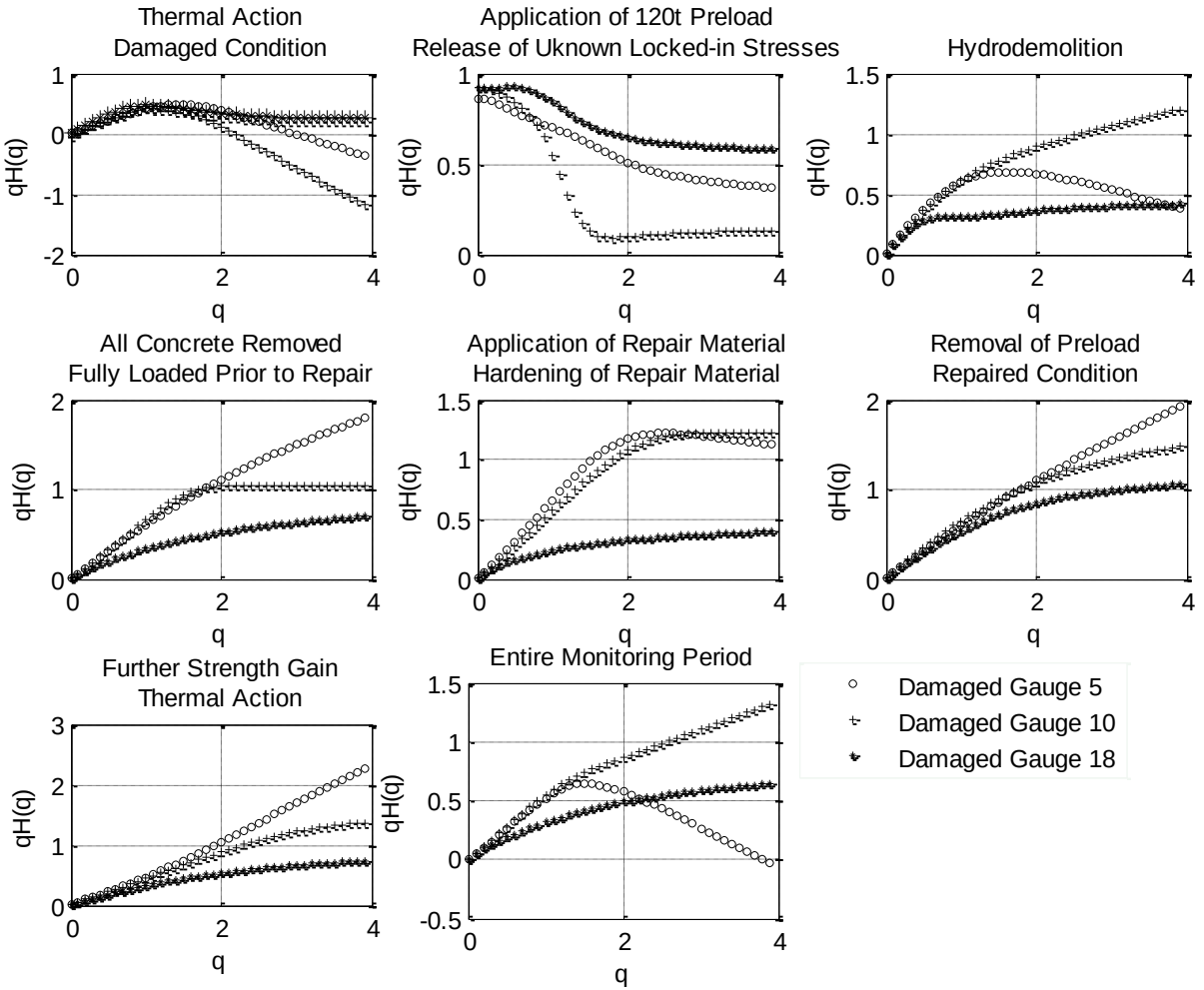
Thermal Action
Damaged Condition
Application of 120t Preload
Release of Uknown Locked-in Stresses
Hydrodemolition
All Concrete Removed
Fully Loaded Prior to Repair
Application of Repair Material
Hardening of Repair Material
Removal of Preload
Repaired Condition
Further Strength Gain
Thermal Action
Entire Monitoring Period
qH(q)
q
Damaged Gauge 5
Damaged Gauge 10
Damaged Gauge 18

Figure 9

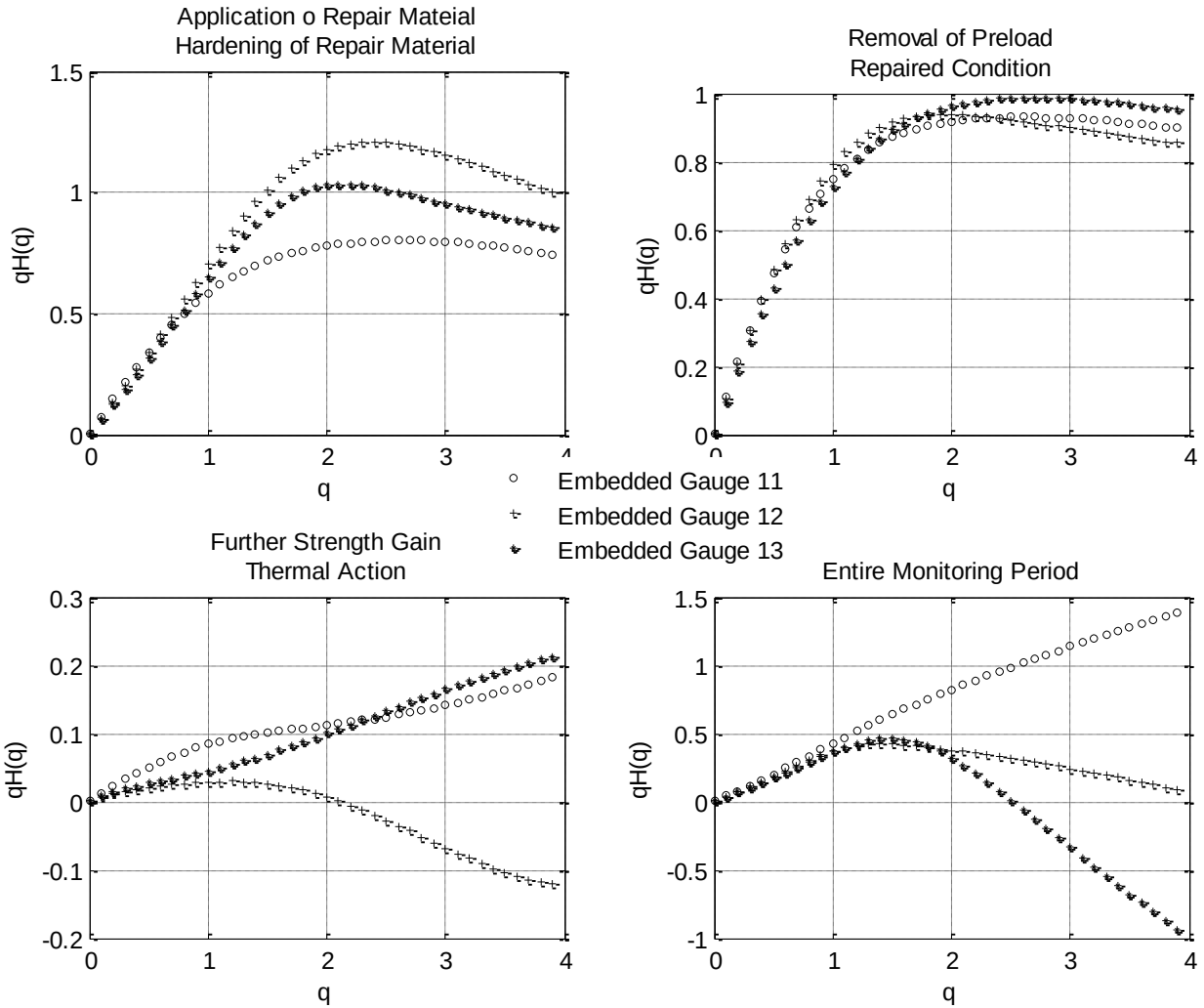
Application o Repair Mateial
Hardening of Repair Material
Removal of Preload
Repaired Condition
Further Strength Gain
Thermal Action
Entire Monitoring Period
qH(q)
q
Embedded Gauge 11
Embedded Gauge 12
Embedded Gauge 13

Figure 10

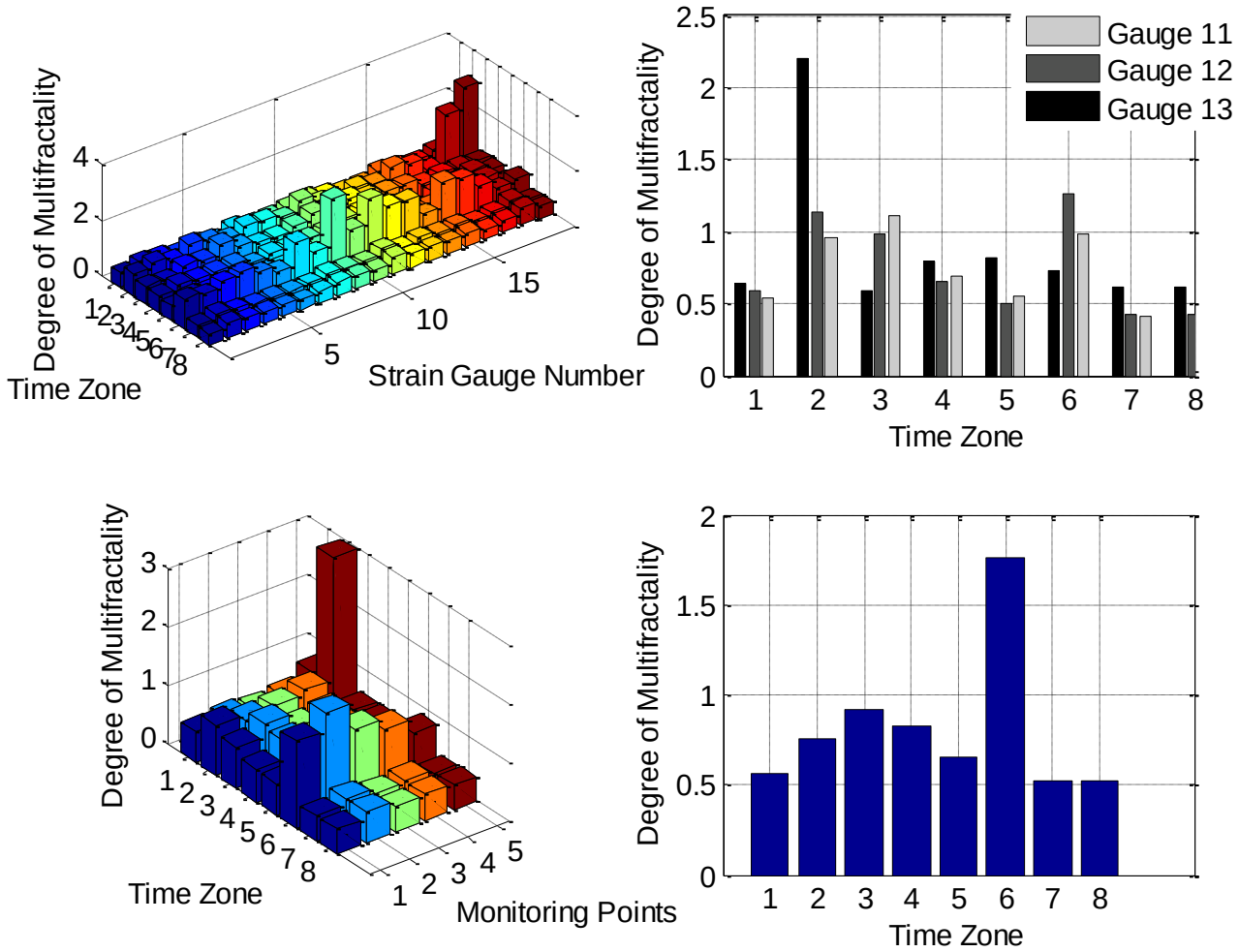
Degree of Multifractality
Time Zone
Strain Gauge Number
Gauge 11
Gauge 12
Gauge 13
Degree of Multifractality
Time Zone
Degree of Multifractality
Time Zone
Monitoring Points
Degree of Multifractality
Time Zone

Figure 11

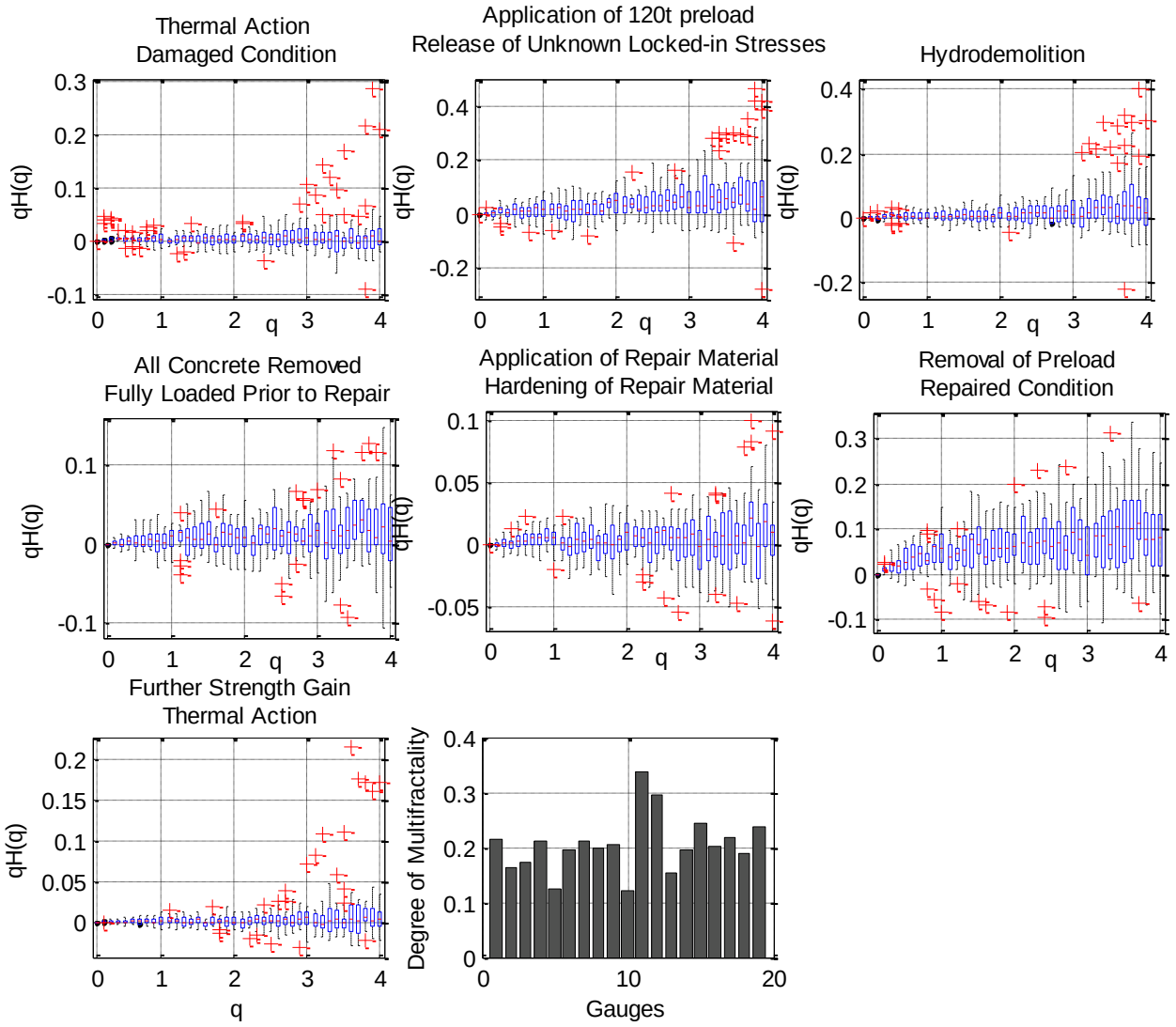
Thermal Action
Damaged Condition
Application of 120t preload
Release of Unknown Locked-in Stresses
Hydrodemolition
All Concrete Removed
Fully Loaded Prior to Repair
Application of Repair Material
Hardening of Repair Material
Removal of Preload
Repaired Condition
Further Strength Gain
Thermal Action
qH(q)
q
Degree of Multifractality
Gauges

Figure 12

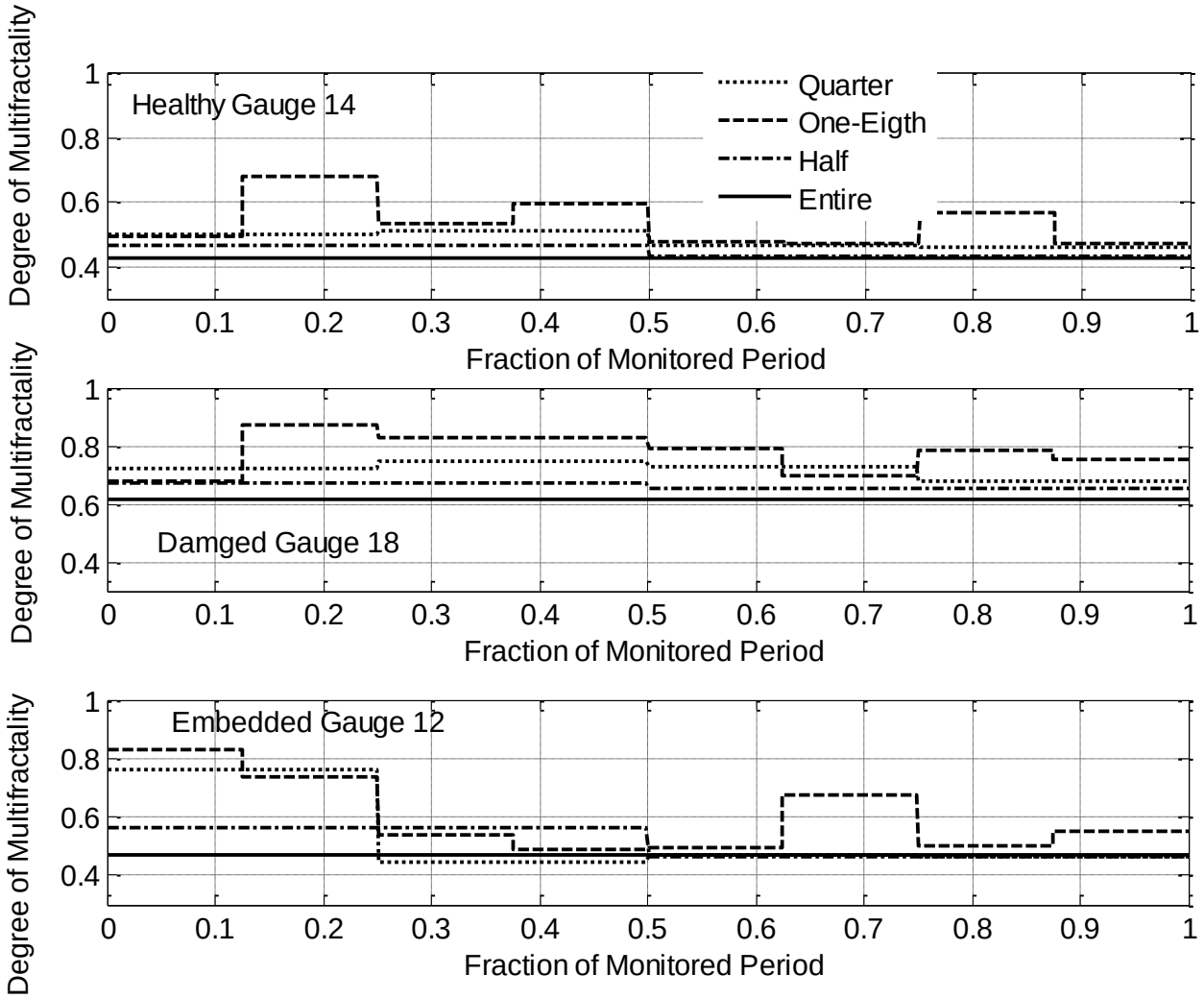
Degree of Multifractality
Healthy Gauge 14
Quarter
One-Eigth
Half
Entire
Fraction of Monitored Period
Damged Gauge 18
Embedded Gauge 12
0
0.1
0.2
0.3
0.4
0.5
0.6
0.7
0.8
0.9
1
0.4
0.6
0.8

Figure 13

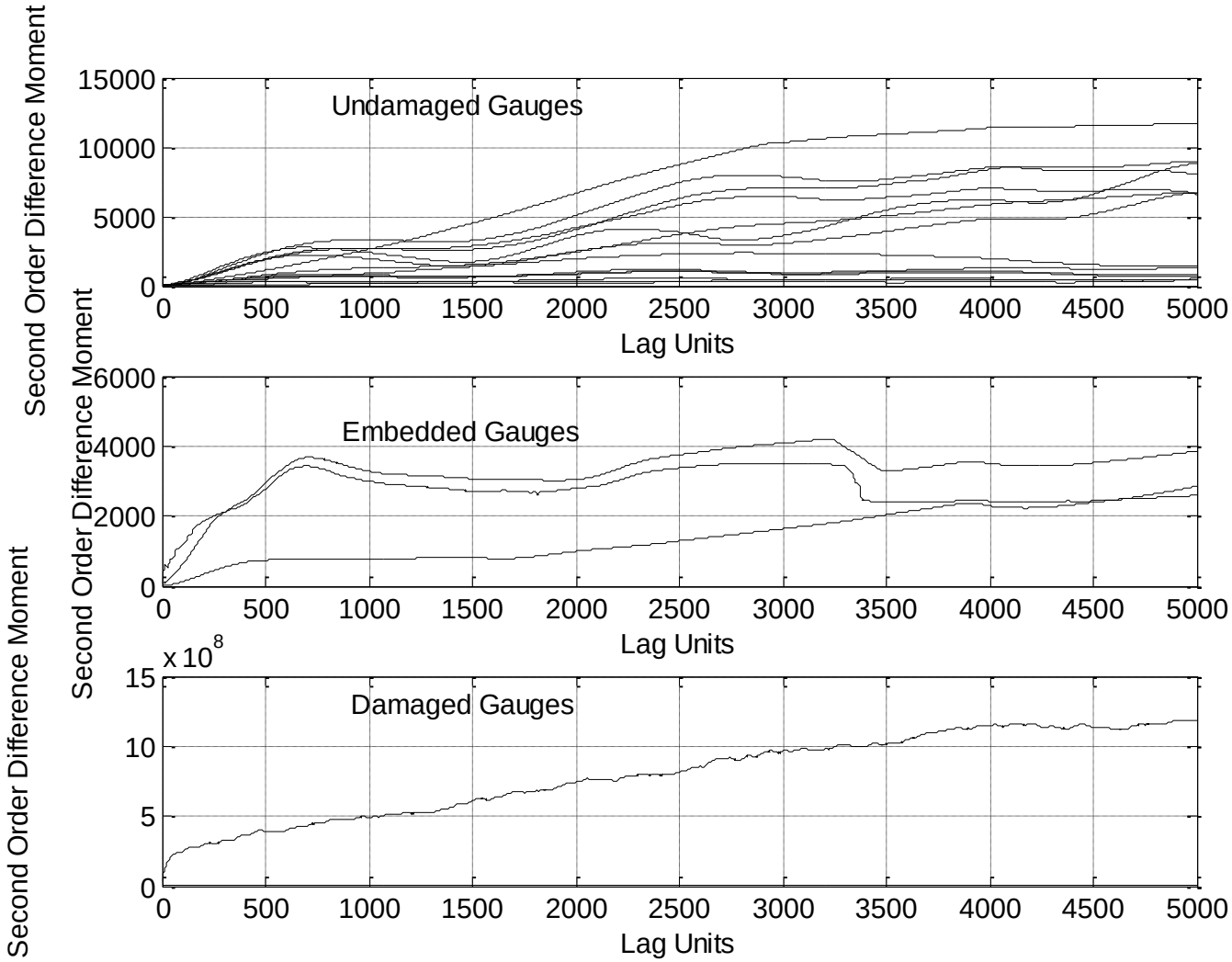
Undamaged Gauges
Second Order Difference Moment
15000
10000
5000
0
0 500 1000 1500 2000 2500 3000 3500 4000 4500 5000
Lag Units
Embedded Gauges
Second Order Difference Moment
6000
4000
2000
0
0 500 1000 1500 2000 2500 3000 3500 4000 4500 5000
Lag Units
Damaged Gauges
Second Order Difference Moment
x 10^8
15
10
5
0
0 500 1000 1500 2000 2500 3000 3500 4000 4500 5000
Lag Units

Figure 14